

Article

Petrographical and Geochemical Study of Syn-Rift Sediments, Pranhita-Godavari Intracratonic Gondwana Basin, India: Genesis and Paleo-Environmental Implications

Sanghita Dasgupta ¹, Santanu Banerjee ^{1,*} and Parthasarathi Ghosh ²

¹ Department of Earth Sciences, Indian Institute of Technology Bombay, Powai, Mumbai 400076, India; sangu.dg@gmail.com

² Geological Studies Unit, Indian Statistical Institute, 203 B.T. Road, Kolkata 700108, India; pghosh@isical.ac.in

* Correspondence: santanu@iitb.ac.in

Abstract: The approximately 2 km thick fluvio-lacustrine deposits of Pranhita-Godavari Gondwana syn-rift basin, ranging in age from 235 to 196 Ma, track the compositional changes from the Middle Triassic to Early Jurassic. Mineralogical and geochemical investigations, as well as paleocurrent data of the siliciclastic deposits of the four conformable formations—Yerrapalli, Bhimaram, Maleri and Dharmaram—trace the source of sediments to the south and southwest of the Gondwana basin. The dominance of arkosic to sub-arkosic sandstones in all the formations suggests mostly felsic sources. The high value of Zr/Sc, as well as a high content of Hf, reflects the addition of zircon by sediment recycling. The index of compositional variability (ICV) and chemical index of alteration (CIA) values of these Gondwana samples suggest intermediate weathering of Proterozoic shales, granites and gneisses. The concentration of Cr and Ni, ratios of Eu/Eu* and (Gd_N/Yb_N) suggest a dominant post-Archean source. The insignificant variation in ICV and CIA values across the studied Mesozoic formations corroborates the continuation of syn-rift tectonics of the Pranhita-Godavari Gondwana basin since the Late Paleozoic. Sandstone samples show a gradual shift from arkose to subarkose in Yerrapalli, Barakar and Maleri formations, and to sublithic arenite sandstones in the younger Dharmaram formation, indicating recycling. However, the insignificant variation of feldspar and/or quartz content throughout these Mesozoic formations suggests lesser tectonic activity. The paleocurrent direction, shifting from NNW to NE direction, suggests a change in basin tectonism and/or sediment supply, which is corroborated by mineralogical and geochemical data.

Keywords: major element chemistry; Middle Triassic to Early Jurassic; Pranhita-Godavari syn-Rift Gondwana basin; petrography; provenance



Citation: Dasgupta, S.; Banerjee, S.; Ghosh, P. Petrographical and Geochemical Study of Syn-Rift Sediments, Pranhita-Godavari Intracratonic Gondwana Basin, India: Genesis and Paleo-Environmental Implications. *Geosciences* **2022**, *12*, 230. <https://doi.org/10.3390/geosciences12060230>

Academic Editors: Emilia Le Pera, Consuele Morrone, Angelos G. Maravelis and Jesus Martinez-Frias

Received: 11 January 2022

Accepted: 26 May 2022

Published: 30 May 2022

Publisher's Note: MDPI stays neutral with regard to jurisdictional claims in published maps and institutional affiliations.



Copyright: © 2022 by the authors. Licensee MDPI, Basel, Switzerland. This article is an open access article distributed under the terms and conditions of the Creative Commons Attribution (CC BY) license (<https://creativecommons.org/licenses/by/4.0/>).

1. Introduction

By the Late Jurassic period, East Gondwanaland had started breaking apart from West Gondwanaland, which separated Africa from India–Antarctica [1]. The uplift at the India–Antarctic boundary reached a maximum in the Early Cretaceous, after which India started separating from Antarctica, thus created the modern coastline of eastern India [2]. Madagascar (the connecting link between India and Africa) rifted apart from India during the Late Cretaceous and the Indian Ocean opened up all along India's western margin [2]. These tectonic events caused the tilting of the east-Indian basins towards SE [3,4]. The sedimentary strata that deposited in different areas of peninsular India, mainly in four intracratonic basins, i.e., Pranhita-Godavari, Damodar, Satpura, and Son-Mahanadi, between Permo-Carboniferous and Early Jurassic time (290–182 Ma) are referred to as the Indian Gondwanas, and the corresponding sediments as the Gondwana sediments [5–9]. The provenance study and mineralogical and geochemical evolution of these riftogenic Gondwana sediments deposited in these four basins is conspicuously under-represented in the literature, except for the Satpura basin [10–12]. These Gondwana sediments are

essentially half-grabens along pre-existing zones of weakness in the Precambrian basement and contain fluvial deposits. These basins witnessed a reversal in the paleodrainage pattern during the Mesozoic time. However, very few provenance studies record the paleodrainage reversal.

Detrital modes of sandstone suites bear the imprints of tectonic settings of the provenance [13–17]. Quantitative detrital mode, calculated from point counts of thin sections, is useful to infer the sandstone provenance [17–21]. The geochemistry of mudstone supplements the provenance interpretations made by modal analysis of associated sandstone [22]. Ratios of trace elements and major oxides serve as proxies for tectonic setting, weathering and recycling [23–28].

In this context, the Pranhita-Godavari intracratonic Gondwana Basin is the target of this study. It preserves the most continuous sedimentary history from Permian to Cretaceous time, recording the evolution of syn-rift tectonic activity. Earlier researchers have not published any geochemical or petrological data on any formations of the Pranhita-Godavari Gondwana basin. Detailed study has only been conducted with reference to stratigraphy, palaeontology and sedimentology (for Maleri, upper Dharmaram and Lower Kota formations), with no work regarding the provenance of these sediments all throughout the Pranhita-Godavari Basin [29]. Thus, the source of a ~4–5 km thick pile of sedimentary deposit is yet to be established.

The present work deals with the petrographical and geochemical investigation of Middle Triassic to early Early Jurassic sandstone and mudstone of the Pranhita-Godavari syn-rift basin. The objectives of this present study are to (i) identify the composition of the source rock, (ii) highlight the paleo-weathering and recycling of the sediment deposited during early the Middle Triassic to early Early Jurassic and (iii) update the tectonic setting of the basin and to record reversal of paleoslope. To fulfill the objectives, we present detailed modal analysis of sandstone and geochemical characterization of mudstone.

2. Geological Background

The paleoposition of India during the Triassic to Jurassic was 20° S to 40° S and 50° E to 30° E [29]. India, along with the other continents of the southern hemisphere, was part of the supercontinent Gondwanaland until its break-up during Jurassic–Early Cretaceous time [30]. A NW-SE trending Neoproterozoic rift-related suture is sandwiched between the Dharwar and Bastar cratonic nuclei [9,31]. The Pranhita-Godavari basin records repeated opening and closing of the rift for about 1600 m.y. from 1.7 to ~0.15 Ga [31]. The eastern margin of the rift was the footwall block during the Mesozoic [9,32,33]. A well-developed axial drainage system existed on the Proterozoic basement at the hanging wall block along the southwestern basin margin, starting as early as 1700 my [31]. The Gondwana deposits overlie the Proterozoic rocks of the Pranhita-Godavari Basin with an unconformity [31,34]. This NW-SE axial trend is expected to continue through much of the area now covered by Late Cretaceous Deccan volcanics [35–37].

The Gondwana basin fill occurs as an elongated NW-SE linear outcrop belt between Proterozoic and Archean basement rocks that constituted the rift shoulders [31]. Axes of the Proterozoic and Gondwana rift systems remained broadly similar [31,35]. The Pranhita-Godavari Basin has witnessed the reversal of paleoslope from a northwesterly to southeasterly direction due to regional upliftment prior to the Madagascar rifting event in the Late Cretaceous [9,32,37]. The focus of this study is the Mesozoic succession comprising the Yerrapalli, Bhimaram, Maleri and Dharmaram formations, in the ascending order of the Pranhita-Godavari Gondwana basin (Table 1; [38–40]). The Yerrapalli and Maleri formations represent part of the Triassic redbed succession. Sheet-like bodies of cross-stratified sandstone and stratified mudstone predominate these formations. Lenses of cross-bedded carbonate grainstone and marlstone units are subordinate. The Bhimaram formation comprises thick, cross-stratified multi-storied sandstone bodies. The Dharmaram formation consists of thick sandstone at the lower part, whereas the upper part shows an alternation of stratified mudstone, sandstone and carbonate grainstone. The contacts

between the formations are gradational. Existing studies, based on sedimentology and fossil assemblages, indicate semi-arid to humid climatic conditions [29].

Table 1. The stratigraphy of the four formations (discussed in this paper), of the Upper Gondwana succession of the Pranhita-Godavari basin, central India, studied and summarized from [39–41].

	Formation	Lithology	Fossil Content	AGE
Upper Gondwanas	Dharmaram (~400–600 m thick)	Planar and trough cross-bedded coarse sandstone (up to 3–6 m thick co-set, ~30–45% by volume), red mudstone (~30–40% by volume), conglomerate and cross stratified carbonate grainstone (~20–30% by volume) and minor proportion of marl	Continental vertebrates, <i>Unio</i> , Large petrified wood	Early Early Jurassic–Late Triassic
	Maleri (~300–500 m thick)	Dominated by pale red, stratified siltstone (up to 0.5–3 m thick co-set, ~50% by volume), fine to medium cross stratified sandstone (up to 2–5 m thick co-set, ~20% by volume), massive mudstone (up to 1–4 m thick, ~25% by volume), planar and trough cross-bedded carbonate grainstone (~5–8%), minor proportion of marl	Continental vertebrates, <i>Unio</i> , petrified wood	Early Late Triassic (Early Norian–Late Carnian)
	Bhimaram (~400 m thick)	Coarse to medium cross-stratified sandstone (up to 3–8 m thick co-set, ~95% by volume), ferruginous or calcareous in places intercalated with minor proportion of red mudstone	Large petrified wood	Late Middle Triassic (Ladinian)
	Yerrapalli (~200 to 500 m thick)	Red and violet mudstone (~70% by volume) with gypsum, laminated calcareous sandstone (up to 2–5 m thick, ~25–28% by volume) and cross stratified carbonate grainstone (~3–5% by volume)	Continental vertebrates, very few petrified wood	Early Middle Triassic (Anisian)
Lower Gondwanas Proterozoic and Archean basement rocks				

3. Methods

Field investigation along the banks of rivers and small creeks provided sedimentological attributes of the four formations. The area of study comprises the north-western part of the Pranhita-Godavari Gondwana basin, India (Figure 1). This area lies within the Adilabad district of Telangana and is covered by the Survey of India toposheets, 56M/7, 56M/8, 56M/11 and 56M/12 around Nambal, Dharmaram, Nannial and Annaram (Figure 1A). Paleocurrent directions were measured on outcrops of cross-stratified sandstones and then the overall direction was cross-checked with the data available in the literature. A brief facies analysis is given in Table 2 and field photographs in Figure 2. Forty representative samples from all four stratigraphic units were collected from different stratigraphic levels, out of which 38 sandstone samples for petrographical analyses and 30 mudstone samples for geochemical analyses were considered.

Thin sections were prepared after treating the rock with epoxy resin and hardener. Petrographic analyses were carried out using Leica DM 4500P polarizing microscope attached with Leica DFC420 camera and Leica Image Analysis software (LAS- v4.6, Wetzlar, Germany) at the Department of Earth Sciences, Indian Institute of Technology (IIT) Bombay. Since matrices, siliciclastic cement or porosity were not observed in these Mesozoic sandstone samples, point counting was done using the Gazzi–Dickinson method [18,42]. Carbonate clasts are included in the lithic fragment pool. The samples were stained with sodium cobaltinitrite solution for the identification of K-feldspars (cf. [43]). Since the number of rock/lithic fragments is lower, other discrimination diagrams were not used in this study [44]. On average, three to five hundred points were counted per thin section for modal analysis (Table 3).

Major element analyses of 20 mudstone samples were carried out using the heavy absorber fusion technique of [45] (Code- 4C FUS-XRF) method at Activation Laboratories Limited, Ontario, Canada. Powdered samples of 0.25 gm (<63 µm) were mixed with 0.75 g lithium metaborate (LiBO₂) and 0.50 g of lithium tetraborate (LiB₄O₇) in a platinum

crucible and fused in a muffle furnace at 1050 °C for 10 min. The crucible containing the fusion bead was immersed in 75 mL of 1 N HCl in a 100 mL glass beaker and then magnetically stirred for 1 h until the fusion bead dissolved completely. The sample volume was then increased up to 100 mL in a volumetric flask. Five mL of this solution was diluted to 50 mL with distilled water and used for the analysis. USGS standards, MAG-1, SBC-1, SCo-1 and SCo-2 were used for the analysis. Prior to fusion, the loss on ignition (LOI) was determined after heating 1 g of a powdered sample at 1000 °C for 2 h. The trace element concentrations of mudstone samples were determined by Perkin-Elmer SCIEX Model ELAN DRC II ICP-Mass Spectrometer using the 'Open Acid Digestion Technique' with PTFE teflon beakers at the National Geophysical Research Institute (NGRI), Hyderabad, India. For each sample, two to three replicate analyses were carried out in order to check that precision and accuracy were within acceptable limits. The precision was <5% relative standard deviation. The internal standard used was 103 Rh. Analytical details are provided in Balaram and Rao [46]. Major oxide trace element concentrations and their ratios were used to prepare binary and ternary plots (data given in Tables 4–7). The major oxide concentrations of the Mesozoic mudstone samples were normalized against Post-Archean average Australian shale (PAAS [47]) and upper continental crust (UCC [48]). The trace element concentration was normalized with respect to the average UCC. Europium anomaly was calculated as $\text{Eu}/\text{Eu}^* = (\text{Eu})\text{CN}/(\sqrt{(\text{Sm})\text{CN} \times (\text{Gd})\text{CN}})$, where $\text{Eu}^* = (\text{Sm} + \text{Gd})/2$ (formula used from McLennan 1989). The REE concentrations of the Mesozoic mudstone samples were normalized against chondrite, PAAS and UCC (chondrite values taken from [47]). The degree of chemical weathering of source rocks was calculated from the chemical index of alteration (CIA: [49]) using the formula

$$\text{CIA} = [n\text{Al}_2\text{O}_3 / (n(\text{Al}_2\text{O}_3) + n(\text{CaO})^* + n(\text{Na}_2\text{O}) + n(\text{K}_2\text{O}))] \times 100, \text{ (in molecular proportions).}$$

where CaO* is the amount incorporated in the silicate fraction of the rock. The higher CIA values represent higher degrees of weathering.

The index of compositional variability (ICV) is a measure of the abundance of alumina relative to the other major cations and also reflects the maturity of the source material of sedimentary rocks [54]. It is defined as

$$\text{ICV} = (n(\text{Fe}_2\text{O}_3) + n(\text{K}_2\text{O}) + n(\text{Na}_2\text{O}) + n(\text{CaO}^*) + n(\text{MgO}) + n(\text{MnO}) + n(\text{TiO}_2)) / n(\text{Al}_2\text{O}_3).$$

Table 2. A brief facies analysis (mainly the siliciclastics) and their main characteristics, in relation to sedimentary structures, depositional environments and appearance in the four formations (discussed in this paper) of the Upper Gondwana succession of the Pranhita-Godavari basin, central India.

Facies	Description	Sedimentary Structures	Depositional Process	Interpretation	Appearance
F1—Parallel laminated sandy siltstone	Laminae thickness 1–5 mm. Stratification defined by variation in proportion of mud aggregates. Tabular sets (30–70 cm) and wedge-shaped sets (10–50 cm) present.	Plane-parallel to low-angle (<3°) laminae.	Low to mid energy, unidirectional traction sedimentation.	Plane beds formed under both upper and lower flow regimes.	Mainly in Yerrapalli and Maleri formations, minor in the Dharamaram formation.
F2—Ripple laminated silt (mud aggregates) to very fine sandstone	Set thickness 0.5–1.2 cm. Wavy lamination and combined-flow ripples present in topset laminae.	Current-ripple cross-laminated. Both planar and trough-shaped foresets.	Low energy, unidirectional traction sedimentation.	Migration of straight-crested and curved-crested ripples under lower flow regime.	Essentially in Yerrapalli and Maleri formations.
F3—Massive mudstone	Silt (~30%), very-fine-sand-size quartz and feldspar grains (~5%), rest red clay. Pedogenic features such as drab-haloed root traces, wedge-shaped peds, mudcracks and rhizocretions present.	Massive. Faint traces of current- and climbing ripple cross lamination in places.	Suspension deposition during flood events.	Fine grained clastics deposited in low-energy environment and modified due to pedogenesis.	Mostly in Yerrapalli formation, occur as paleosols (thickness 3–5 m) in Maleri formation, occur as lenses in Dharmaram formation.
F4—Marl	Bed thickness avg. 5–20 cm; max. 1.5 m. Lateral extent 8–20 m. Alternation of micrite, microspar, and calcareous clay-rich laminae. Shells of aquatic invertebrates and desiccation cracks present.	Thinly laminated (1–5 mm).	Carbonate precipitation.	Deposition of limemud in small, shallow and ephemeral water bodies.	Occur as thin sheets in Maleri and Dharmaram formations.
F5—Cross stratified carbonate grainstone	Medium-sand- to granule-size calcareous grains admixed with silt- to fine-sand-size mud aggregates and other siliciclastic grains. Fossils: freshwater bivalve (<i>Unio</i>), aquatic, semiaquatic vertebrates (bone fragments), and articulated ostracod shells.	Planar (5–35 cm set thickness) and trough (~10 cm set thickness) cross-bedding.	High energy traction currents, unidirectional migration of 2D and 3D sand dunes.	An admixture of carbonate and siliciclastic grains transported as straight-crested and curved crested dunes.	Lensoid bodies in ascending order of occurrence from Yerrapalli-Maleri-Bhimaram-Dharmaram formations.

Table 2. Cont.

Facies	Description	Sedimentary Structures	Depositional Process	Interpretation	Appearance
F6—Parallel laminated very fine to fine grained sandstone	Alternating white and red laminae defined by contrast in grain size as well as by the proportion of mud aggregates in the framework. Fine-sand-size red mud aggregates dominate redish laminae. Sand-size quartz and feldspar grains dominate white laminae.	Lamina thickness 1–5 mm thick, lateral extent 10 cm–2.5 m. Plane-parallel and low-angle (<5°) lamination. Parting lineation on laminae surfaces.	Low energy, unidirectional traction sedimentation.	Plane beds formed in shallow, upper-flow-regime conditions.	Occur as thin sheets in Yerrapalli and co-sets in Maleri formation. Bhimaram and Dharmaram formations have more thicker bodies.
F7—Cross stratified fine to coarse grained sandstone	Set thickness ~15–40 cm, up to 70 cm.	Planar and trough cross-bedding.	High energy traction currents, unidirectional migration of 2D and 3D sand dunes.	Migration of straight-crested and curved-crested sandy dunes.	Minor in Yerrapalli and Maleri, whereas major in Bhimaram and Dharmaram formations.
F8—Ripple laminated fine to very fine sandstone	Set thickness, 0.5–1.5 cm; lateral extent 20–50 cm.	Current-ripple cross-lamination.	Low energy, unidirectional traction sedimentation.	Migration of straight-crested and curved-crested ripples under lower flow regime.	Occur in all four formations.
F9—Medium grained massive sandstone	Lenses have steep margins, concave-up basal surface, internal stratification (where present) becomes progressively gentler from the sides to the centers of the lenses.	Lenses of massive sandstone. Thickness 5–30 cm, lateral extent 10–50 cm.	Rapid suspension fallout.	In-fills of erosional depressions. Either filled gradually from side, or rapidly, thereby obliterating structures due to rapid fluid escape after deposition.	Occur in all four formations.

Table 3. Results of petrographic and modal analyses of sandstone samples of Yerrapalli, Bhimaram, Maleri and Dharmaram formations.

Sample No.	Formation	Qm	Qp(2–3)	Qp(>3)	Qp(>10)	Total Qp	Total Q(Qm + Qp)	F(K)	RF(S)	Bt	HM	Total Count	QFR%			QmFLt%		
													Q	F	R	Qm	F	Lt
Dh 158/11-12	Dharmaram	302	15	3	0	18	320	79	5	0	8	412	79.21	19.55	1.24	74.75	19.55	5.69
Dh 166/11-12	Dharmaram	321	18	4	2	24	345	70	36	1	2	454	76.50	15.52	7.98	71.18	15.52	13.30
Dh 153/11-12	Dharmaram	279	16	2	0	18	297	73	7	0	6	383	78.78	19.36	1.86	74.01	19.36	6.63
Dh 162/11-12	Dharmaram	297	10	1	3	14	311	61	11	0	39	422	81.20	15.93	2.87	77.55	15.93	6.53
Dh 132/11-12	Dharmaram	289	9	0	1	10	299	56	10	0	43	408	81.92	15.34	2.74	79.18	15.34	5.48
Dh 133/11-12	Dharmaram	325	7	0	5	12	337	54	16	0	1	408	82.80	13.27	3.93	79.85	13.27	6.88
Dh 167/11-12	Dharmaram	249	10	7	2	19	268	9	21	2	0	300	89.93	3.02	7.05	83.56	3.02	13.42
Dh 151/11-12	Dharmaram	225	4	2	0	6	231	46	39	0	10	326	73.10	14.56	12.34	71.20	14.56	14.24

Table 3. Cont.

Sample No.	Formation	Qm	Qp(2–3)	Qp(>3)	Qp(>10)	Total Qp	Total Q(Qm + Qp)	F(K)	RF(S)	Bt	HM	Total Count	QFR%			QmFLt%		
													Q	F	R	Qm	F	Lt
Dh 161/11-12	Dharmaram	244	0	8	0	8	252	30	0	0	21	303	89.36	10.64	0.00	86.52	10.64	2.84
Dh 149/11-12	Dharmaram	540	0	6	0	6	546	317	6	10	6	885	62.83	36.48	0.69	62.14	36.48	1.38
411A	Maleri	445	32	5	3	40	485	15	0	0	72	572	97.00	3.00	0.00	89.00	3.00	8.00
Ma39_12-13	Maleri	335	45	10	5	60	395	100	5	0	44	544	79.00	20.00	1.00	67.00	20.00	13.00
Ma61_12-13	Maleri	405	39	15	6	60	465	30	5	0	56	556	93.00	6.00	1.00	81.00	6.00	13.00
Ma62_12-13	Maleri	340	28	14	3	45	385	110	5	0	34	534	77.00	22.00	1.00	68.00	22.00	10.00
Ma65_12-13	Maleri	360	54	12	4	70	430	65	5	0	20	520	86.00	13.00	1.00	72.00	13.00	15.00
Ma108_11-12	Maleri	350	6	3	1	10	360	140	0	1	26	527	72.00	28.00	0.00	70.00	28.00	2.00
Ma121_11-12	Maleri	305	9	4	2	15	320	180	0	0	33	533	64.00	36.00	0.00	61.00	36.00	3.00
Ma126_11-12	Maleri	330	9	8	3	20	350	150	0	0	31	531	70.00	30.00	0.00	66.00	30.00	4.00
Ma188_11-12	Maleri	330	39	6	5	50	380	120	0	2	27	529	76.00	24.00	0.00	66.00	24.00	10.00
Ma103_11-12	Maleri	355	31	14	0	45	400	100	0	0	38	538	80.00	20.00	0.00	71.00	20.00	9.00
Ma106_11-12	Maleri	325	26	6	3	35	360	135	5	0	26	526	72.00	27.00	1.00	65.00	27.00	8.00
Ma196_11-12	Maleri	330	25	11	4	40	370	125	5	1	30	531	74.00	25.00	1.00	66.00	25.00	9.00
Ma124_11-12	Maleri	315	5	2	1	8	323	185	0	0	18	526	63.58	36.42	0.00	62.01	36.42	1.57
421	Maleri	300	51	9	0	60	360	135	5	1	10	511	72.00	27.00	1.00	60.00	27.00	13.00
Ma41_12-13	Maleri	325	44	13	8	65	390	105	5	0	21	521	78.00	21.00	1.00	65.00	21.00	14.00
Ma37_12-13	Maleri	305	22	14	9	45	350	145	5	0	16	516	70.00	29.00	1.00	61.00	29.00	10.00
Ma40_12-13	Maleri	370	9	6	5	20	390	110	0	2	42	544	78.00	22.00	0.00	74.00	22.00	4.00
Ma23_12-13	Maleri	330	33	16	1	50	380	120	0	0	22	522	76.00	24.00	0.00	66.00	24.00	10.00
Ma6_14-15	Maleri	330	29	16	0	45	375	120	5	0	19	519	75.00	24.00	1.00	66.00	24.00	10.00
Ma9_14-15	Maleri	365	20	13	2	35	400	95	5	1	25	526	80.00	19.00	1.00	73.00	19.00	8.00
Bh 201/11-12	Bhimaram	332	9	2	0	11	343	68	5	0	70	486	82.45	16.35	1.20	79.81	16.35	3.85
Bh 118/11-12	Bhimaram	295	11	0	3	14	309	76	7	0	55	447	78.83	19.39	1.79	75.26	19.39	5.36
Bh 191A/11-12	Bhimaram	369	8	0	0	8	377	81	5	2	29	494	81.43	17.49	1.08	79.70	17.49	2.81
Bh187/11-12	Bhimaram	342	12	0	2	14	356	62	8	0	74	500	83.57	14.55	1.88	80.28	14.55	5.16
Yr 177/11-12	Yerrapalli	391	20	1	4	25	416	7	6	0	0	429	96.97	1.63	1.40	91.14	1.63	7.23
Yr 179/11-12	Yerrapalli	355	30	7	3	40	395	323	0	5	111	834	55.01	44.99	0.00	49.44	44.99	5.57
Yr 180/11-12	Yerrapalli	461	0	0	0	0	461	338	0	28	84	911	57.70	42.30	0.00	57.70	42.30	0.00
Yr 178/11-12	Yerrapalli	411	4	0	0	4	415	248	9	0	34	706	61.76	36.90	1.34	61.16	36.90	1.93

Qm—monocrystalline quartz, Qp(2–3)—polycrystalline quartz—2–3 sub-crystals with tectonic fabric, Qp(>3)—polycrystalline quartz—>3 sub-crystals with tectonic fabric, Qp(<10)—polycrystalline quartz—<10 sub-crystals with tectonic fabric, F(K)—K-feldspar, RF(S)—sedimentary lithic fragment of siliciclastic composition, Bt—biotite, HM—heavy mineral, Q—Qm + Qp, R or L—total lithic fragment.

Table 4. Major oxide concentration (wt.%) in mudstone samples of the Yerrapalli, Maleri and Dharmaram formations.

Samples	SiO ₂	Al ₂ O ₃	Fe ₂ O ₃	MnO	MgO	CaO	Na ₂ O	K ₂ O	TiO ₂	P ₂ O ₅	LOI	Total	Al ₂ O ₃ /TiO ₂	ICV	CIA
Dh170/11-12	69.22	15.97	5.16	0.04	0.56	0.17	0.24	0.63	0.97	0.06	7.53	100.60	16.46	0.49	93.89
Dh136/11-12	51.86	16.33	8.83	0.06	2.38	3.07	0.44	2.50	0.74	0.14	13.59	100.10	22.07	1.11	73.10
Ma2/12-13	52.39	16.26	9.43	0.12	2.79	0.54	0.71	2.58	0.73	0.09	14.31	100.20	22.27	1.05	80.94
Ma4/12-13	51.04	14.88	8.06	0.07	2.74	4.36	0.30	2.39	0.70	0.17	15.69	100.80	21.26	1.27	67.85
Ma8/12-13	53.28	15.36	7.97	0.14	2.79	1.66	0.44	2.18	0.76	0.16	14.89	99.86	20.21	1.05	78.21
Ma13/12-13	51.32	16.15	8.62	0.18	2.90	2.26	0.47	2.26	0.72	0.16	15.70	100.80	22.43	1.08	76.40
Ma49/12-13	52.63	13.37	6.05	0.15	2.10	5.89	0.32	2.43	0.64	0.14	15.48	99.88	20.89	1.37	60.75
Ma27/12-13	57.73	15.24	7.46	0.14	2.40	0.93	0.15	2.81	0.68	0.09	12.78	100.70	22.41	0.98	79.67
Ma28/12-13	58.97	15.17	6.67	0.05	2.34	0.57	0.22	2.87	0.64	0.09	11.94	99.87	23.70	0.90	80.56
Ma35/12-13	50.02	16.16	8.68	0.07	2.77	2.92	0.35	2.27	0.71	0.15	15.35	100.00	22.76	1.13	74.47
Ma42/12-13	49.72	15.86	8.24	0.08	2.73	2.45	0.59	2.39	0.69	0.14	17.17	100.30	22.99	1.10	74.50
Ma50/12-13	54.66	15.44	7.07	0.05	2.60	1.52	0.41	2.04	0.76	0.16	15.07	100.40	20.32	0.97	79.55
Ma109/11-12	61.63	14.01	7.76	0.06	1.78	0.31	0.56	2.80	0.91	0.09	9.76	99.68	15.40	1.01	79.24
Ma113/11-12	52.98	13.48	5.36	0.12	2.43	6.19	0.20	2.02	0.65	0.12	15.96	100.30	20.74	1.32	61.58
Ma141/11-12	65.79	14.20	7.50	0.02	1.51	0.23	0.58	1.97	0.82	0.10	7.40	100.10	17.32	0.89	83.63
Ma173/11-12	54.75	15.02	7.14	0.07	2.65	2.83	0.55	2.64	0.68	0.14	12.73	99.32	22.09	1.11	71.39
Ma193/11-12	54.82	15.28	7.14	0.04	2.64	1.88	0.51	2.59	0.72	0.15	14.43	100.40	21.22	1.03	75.42
Ma199/11-12	52.51	14.37	7.34	0.12	2.57	4.08	0.34	2.06	0.71	0.14	15.91	100.20	20.24	1.20	68.92
Yr148/11-12	63.05	16.59	7.36	0.01	0.79	0.57	0.24	0.59	0.79	0.12	9.79	100.50	21.00	0.66	92.22
Yr183/11-12	52.63	15.18	8.38	0.07	2.72	2.94	0.42	3.20	0.70	0.16	14.16	100.60	21.69	1.21	69.83

Table 5. Trace element concentration (ppm) in mudstone samples of Yerrapalli, Bhimaram, Maleri and Dharmaram formations.

Sample	Sc	V	Cr	Co	Ni	Cu	Zn	Ga	Y	Zr	Nb	Hf	Ta	Th	U	Rb	Sr	Cs	Ba	Pb
Dh 136/11-12	15.20	127.16	73.33	35.29	85.98	62.09	161.31	27.30	43.21	2893.59	14.12	57.65	1.05	18.58	5.47	163.31	153.54	9.47	288.51	46.24
Dh 171/11-12	12.88	125.11	72.51	16.90	80.58	52.60	164.65	29.78	48.06	5854.69	14.82	118.70	1.81	17.79	8.98	127.95	157.78	13.33	361.99	54.17
Dh 164/11-12	34.96	327.69	74.02	18.02	44.69	61.76	90.85	40.09	46.04	6389.78	16.90	132.35	2.32	33.39	9.78	32.15	123.81	8.83	405.95	165.29
Dh 169/11-12	30.73	98.96	73.38	8.04	31.22	37.62	240.52	40.09	28.72	4926.51	19.12	98.88	2.20	32.81	6.89	23.31	110.95	6.94	281.46	70.41
Dh 170/11-12	12.71	115.88	71.32	41.76	50.65	48.57	94.21	25.25	36.70	3015.54	17.78	62.98	1.98	24.46	6.41	59.65	84.93	8.54	240.37	64.78
Dh 172/11-12	9.77	60.78	72.35	28.59	72.97	37.78	109.61	14.15	31.54	1534.99	9.67	30.51	1.40	16.77	3.52	94.72	135.51	6.97	243.21	46.54
Dh 114/11-12	14.36	123.30	73.61	22.90	70.78	53.34	143.57	24.46	45.06	2246.87	14.41	45.77	1.45	17.32	4.98	159.35	136.74	7.46	503.31	48.47
Ma 141/11-12	14.39	136.71	67.35	31.05	77.99	47.26	125.16	31.74	44.84	6366.35	15.74	135.94	2.22	21.97	10.49	157.03	125.28	17.53	384.89	62.79
Ma 113/11-12	13.92	114.00	74.29	21.30	82.32	51.97	156.27	32.38	53.42	5718.42	15.05	120.80	1.93	20.49	8.88	129.51	211.62	11.38	443.10	52.55
Ma 128/11-12	14.28	109.46	76.66	19.84	77.40	58.72	149.60	26.01	45.87	2844.35	14.81	56.03	1.33	18.04	5.60	143.12	150.22	7.62	498.19	49.73
Ma 173/11-12	12.20	84.16	70.42	14.99	53.52	50.69	135.79	25.60	43.00	3538.75	13.73	74.10	1.40	17.74	6.31	131.07	146.90	8.87	1587.85	79.11
Ma 193/11-12	13.52	106.02	70.80	16.92	60.13	54.48	111.93	29.25	44.97	4333.92	15.59	91.28	1.61	19.03	6.74	147.90	142.12	10.14	276.60	66.90
Ma 194/11-12	15.30	115.61	73.66	16.29	73.16	58.48	129.12	33.36	47.54	5583.49	16.40	110.56	1.71	19.10	7.63	154.66	159.37	11.84	197.26	68.41
Ma 199/11-12	12.87	77.93	73.71	18.74	53.19	45.23	104.48	24.43	51.68	2837.77	14.01	55.14	1.54	16.92	5.48	122.19	171.43	7.28	475.43	61.13
Ma 200/11-12	15.64	122.83	68.36	16.05	61.48	49.71	116.22	29.35	47.83	3384.46	15.37	71.51	1.52	17.45	5.85	150.11	153.71	9.16	171.07	60.55
Ma 8/9-10	14.76	138.12	70.43	23.94	72.66	61.04	129.14	27.10	45.08	3255.77	14.49	67.21	1.30	17.79	5.31	124.06	142.64	7.49	300.48	60.35
Ma 109/11-12	11.68	71.16	67.08	18.69	60.82	50.01	149.34	20.94	38.05	2253.16	15.93	49.03	1.58	28.17	4.64	134.98	142.55	5.64	601.43	55.47
Ma 104/11-12	13.39	92.33	68.95	15.48	78.62	54.58	149.68	25.19	42.64	3048.90	15.09	65.04	1.52	18.29	5.99	145.24	150.93	8.95	200.49	48.85
Ma 106/11-12	11.95	121.85	67.00	24.36	59.29	54.09	153.04	30.17	40.68	4044.77	15.71	87.86	1.80	26.28	8.37	137.38	149.01	8.06	505.63	57.83
Ma 110/11-12	16.43	140.82	75.51	22.71	78.63	61.43	165.34	27.66	46.48	2405.31	14.48	48.48	1.31	17.04	5.27	149.53	165.40	6.98	159.57	48.71
Ma 9/9-10	15.86	131.25	75.28	24.00	86.88	66.57	187.18	31.58	48.99	4928.87	14.73	96.06	0.84	18.80	7.34	135.16	175.79	9.49	712.82	51.26
Ma 129/11-12	14.46	138.18	72.85	22.35	77.90	56.38	193.80	24.59	48.37	2733.44	13.13	55.00	1.25	20.70	5.02	139.87	136.42	7.31	271.85	48.13
Bh 142/11-12	15.41	134.26	70.30	25.69	69.75	61.71	130.16	25.53	43.53	2074.55	13.42	43.45	0.56	19.10	4.13	130.58	143.75	6.11	312.27	67.31
Yr 145/11-12	12.76	118.97	65.76	17.76	55.20	46.73	201.61	28.36	44.12	4399.52	17.64	95.21	2.08	19.50	7.75	98.12	154.81	11.95	149.78	59.04
Yr 182/11-12	11.57	82.57	69.97	15.44	38.24	40.77	113.22	22.11	45.25	2949.18	16.59	60.56	1.71	19.28	5.12	59.49	116.12	7.72	142.13	60.11
Yr 184/11-12	14.74	142.48	69.74	22.86	85.57	51.48	137.99	39.17	117.08	8036.72	18.82	170.36	2.40	21.70	16.70	168.41	158.12	20.21	285.98	64.77
Yr 148 (2)/11-1	13.06	114.66	69.23	10.41	46.69	44.11	168.24	29.10	87.37	3644.22	17.94	77.60	1.95	18.10	8.41	64.85	75.39	9.69	175.98	61.63
Yr 148/11-12	13.25	110.85	69.64	9.60	53.71	49.61	137.84	27.77	89.21	2950.21	18.00	61.34	1.80	17.62	7.71	64.44	91.34	8.92	117.48	60.56
Yr 183/11-12	13.86	102.69	71.61	20.49	72.03	57.50	171.42	27.61	44.35	3707.76	15.24	74.64	1.52	16.30	5.94	163.70	138.67	10.00	260.37	46.54

Table 6. Concentration of rare earth elements (ppm) in the Mesozoic mudstone samples.

Sample	La	Ce	Pr	Nd	Sm	Eu	Gd	Tb	Dy	Ho	Er	Tm	Yb	Lu
Dh 136/11-12	47.26	99.15	9.99	37.88	7.41	1.43	6.99	1.12	6.98	1.61	4.33	0.78	4.07	0.65
Dh 171/11-12	48.15	100.59	10.38	39.96	7.83	1.52	7.20	1.17	7.26	1.68	4.73	0.89	4.83	0.80
Dh 164/11-12	101.31	181.34	16.73	53.75	7.73	1.37	7.57	1.14	7.31	1.72	4.97	0.95	5.28	0.86
Dh 169/11-12	80.42	179.20	18.67	66.75	11.08	1.76	7.68	1.01	5.27	1.15	3.52	0.67	3.91	0.64
Dh 170/11-12	52.30	105.71	10.11	37.06	6.88	1.20	6.16	0.95	5.85	1.37	3.83	0.72	4.02	0.63
Dh 172/11-12	38.80	88.49	8.21	31.10	5.93	1.07	5.43	0.83	4.81	1.07	2.90	0.50	2.62	0.41
Dh 114/11-12	52.21	115.19	11.19	42.69	8.44	1.69	7.66	1.20	7.29	1.66	4.38	0.76	3.97	0.61
Ma 141/11-12	39.22	90.85	8.84	33.86	6.96	1.33	6.55	1.08	7.10	1.72	4.90	0.98	5.36	0.91
Ma 113/11-12	54.74	103.45	11.32	44.17	8.69	1.87	8.13	1.32	8.32	1.97	5.50	1.01	5.59	0.90
Ma 128/11-12	49.16	100.61	10.50	40.07	7.90	1.57	7.25	1.16	7.06	1.63	4.45	0.76	4.07	0.64
Ma 173/11-12	47.42	99.22	10.17	39.34	8.36	2.08	7.21	1.10	6.82	1.56	4.25	0.77	4.07	0.65
Ma 193/11-12	46.88	100.90	10.39	39.90	7.97	1.53	7.33	1.18	7.36	1.68	4.63	0.85	4.61	0.74
Ma 194/11-12	47.02	96.13	10.17	38.82	7.56	1.43	7.11	1.16	7.21	1.68	4.75	0.88	4.71	0.77
Ma 199/11-12	54.04	111.08	11.23	42.63	8.24	1.70	7.71	1.24	7.76	1.80	4.77	0.86	4.43	0.69
Ma 200/11-12	57.36	121.40	12.49	47.64	9.07	1.77	8.61	1.34	8.09	1.81	4.85	0.86	4.43	0.70
Ma 8/9-10	49.30	101.79	10.32	39.79	7.85	1.56	7.47	1.19	7.29	1.68	4.51	0.81	4.31	0.70
Ma 109/11-12	66.82	148.09	14.32	53.83	10.10	1.86	8.74	1.24	6.98	1.50	4.07	0.70	3.75	0.59
Ma 104/11-12	45.81	91.98	10.10	39.49	7.84	1.46	7.24	1.14	7.09	1.61	4.33	0.79	4.16	0.66
Ma 106/11-12	67.35	150.36	14.33	53.80	9.89	1.93	8.76	1.25	7.24	1.64	4.47	0.80	4.30	0.71
Ma 110/11-12	48.29	101.52	10.41	39.99	7.85	1.56	7.48	1.21	7.44	1.70	4.43	0.78	4.04	0.62
Ma 9/9-10	51.91	108.69	11.10	41.96	8.40	1.74	7.48	1.21	7.51	1.75	4.74	0.87	4.66	0.75
Ma 129/11-12	54.44	106.87	10.99	41.81	8.13	1.55	7.54	1.19	7.49	1.74	4.68	0.83	4.31	0.66
Bh 142/11-12	48.92	99.79	10.12	38.83	7.56	1.47	7.11	1.13	6.95	1.63	4.33	0.77	4.12	0.63
Yr 145/11-12	45.42	101.39	10.24	39.05	7.77	1.37	7.28	1.17	7.22	1.66	4.64	0.86	4.64	0.76
Yr 182/11-12	46.27	103.35	10.13	38.73	7.65	1.40	6.99	1.13	7.02	1.64	4.52	0.82	4.35	0.68
Yr 184/11-12	78.64	165.45	16.29	64.51	13.23	2.60	14.05	2.39	16.07	4.05	10.86	1.95	10.05	1.61
Yr 148 (2)/11-12	84.09	177.47	16.44	68.12	14.15	2.94	16.03	2.58	15.95	3.47	8.81	1.52	7.81	1.18
Yr 148/11-12	90.65	190.36	17.77	73.22	15.13	3.12	17.13	2.72	16.17	3.52	8.74	1.48	7.54	1.10
Yr 183/11-12	44.76	97.94	9.85	37.60	7.49	1.50	6.97	1.10	6.91	1.61	4.37	0.80	4.26	0.68

Table 7. Ratios of trace element concentration in the Mesozoic mudstone samples.

Sample	La/Sc	La/Th	Th/Sc	Zr/Sc	ΣREE	Eu/Eu*	Gd _n /Yb _n	LREE/HREE	Cr/V	Zr/Hf	Y/Ni	Th/Co	La _N /Yb _N	La _N /Sm _N
Dh 136/11-12	3.11	2.54	1.22	190	230	0.61	1.39	7.61	0.58	50.19	0.50	0.53	7.86	4.01
Dh 171/11-12	3.74	2.71	1.38	455	237	0.62	1.21	7.24	0.58	49.33	0.60	1.05	6.74	3.87
Dh 164/11-12	2.90	3.03	0.95	183	392	0.55	1.16	12.11	0.23	48.28	1.03	1.85	12.97	8.25
Dh 169/11-12	2.62	2.45	1.07	160	382	0.58	1.59	14.93	0.74	49.82	0.92	4.08	13.89	4.57
Dh 170/11-12	4.12	2.14	1.92	237	237	0.56	1.24	9.02	0.62	47.88	0.72	0.59	8.80	4.78
Dh 172/11-12	3.97	2.31	1.72	157	192	0.58	1.68	9.29	1.19	50.32	0.43	0.59	9.99	4.12
Dh 114/11-12	3.64	3.01	1.21	157	259	0.64	1.56	8.34	0.60	49.09	0.64	0.76	8.88	3.90
Ma 141/11-12	2.73	1.79	1.53	442	210	0.60	0.99	6.29	0.49	46.83	0.57	0.71	4.94	3.55
Ma 113/11-12	3.93	2.67	1.47	411	257	0.68	1.18	6.79	0.65	47.34	0.65	0.96	6.62	3.97
Ma 128/11-12	3.44	2.73	1.26	199	237	0.64	1.45	7.71	0.70	50.76	0.59	0.91	8.17	3.92
Ma 173/11-12	3.89	2.67	1.45	290	233	0.82	1.43	7.74	0.84	47.76	0.80	1.18	7.87	3.57
Ma 193/11-12	3.47	2.46	1.41	321	236	0.61	1.29	7.26	0.67	47.48	0.75	1.12	6.87	3.70
Ma 194/11-12	3.07	2.46	1.25	365	229	0.59	1.22	7.07	0.64	50.50	0.65	1.17	6.75	3.91
Ma 199/11-12	4.20	3.19	1.31	220	258	0.65	1.41	7.77	0.95	51.47	0.97	0.90	8.25	4.13
Ma 200/11-12	3.67	3.29	1.12	216	280	0.61	1.58	8.09	0.56	47.33	0.78	1.09	8.75	3.98
Ma 8/9-10	3.34	2.77	1.21	221	239	0.62	1.40	7.47	0.51	48.44	0.62	0.74	7.72	3.95
Ma 109/11-12	5.72	2.37	2.41	193	323	0.61	1.89	10.64	0.94	45.96	0.63	1.51	12.05	4.17
Ma 104/11-12	3.42	2.50	1.37	228	224	0.59	1.41	7.22	0.75	46.88	0.54	1.18	7.44	3.68
Ma 106/11-12	5.64	2.56	2.20	339	327	0.63	1.65	10.14	0.55	46.04	0.69	1.08	10.58	4.29
Ma 110/11-12	2.94	2.83	1.04	146	237	0.62	1.50	7.51	0.54	49.61	0.59	0.75	8.08	3.87
Ma 9/9-10	3.27	2.76	1.19	311	253	0.67	1.30	7.67	0.57	51.31	0.56	0.78	7.53	3.89
Ma 129/11-12	3.76	2.63	1.43	189	252	0.61	1.42	7.82	0.53	49.70	0.62	0.93	8.54	4.22
Bh 142/11-12	3.18	2.56	1.24	135	233	0.61	1.40	7.70	0.52	47.74	0.62	0.74	8.03	4.07
Yr 145/11-12	3.56	2.33	1.53	345	233	0.56	1.27	7.22	0.55	46.21	0.80	1.10	6.62	3.68
Yr 182/11-12	4.00	2.40	1.67	255	235	0.58	1.30	7.59	0.85	48.70	1.18	1.25	7.18	3.81
Yr 184/11-12	5.34	3.62	1.47	545	402	0.58	1.13	5.54	0.49	47.17	1.37	0.95	5.29	3.74
Yr 148 (2)/11-12	6.44	4.65	1.39	279	421	0.60	1.66	6.28	0.60	46.96	1.87	1.74	7.28	3.77
Yr 148/11-12	6.84	5.14	1.33	223	449	0.59	1.84	6.63	0.63	48.10	1.66	1.84	8.13	3.76
Yr 183/11-12	3.23	2.75	1.18	267	226	0.64	1.33	7.41	0.70	49.68	0.62	0.80	7.10	4.10

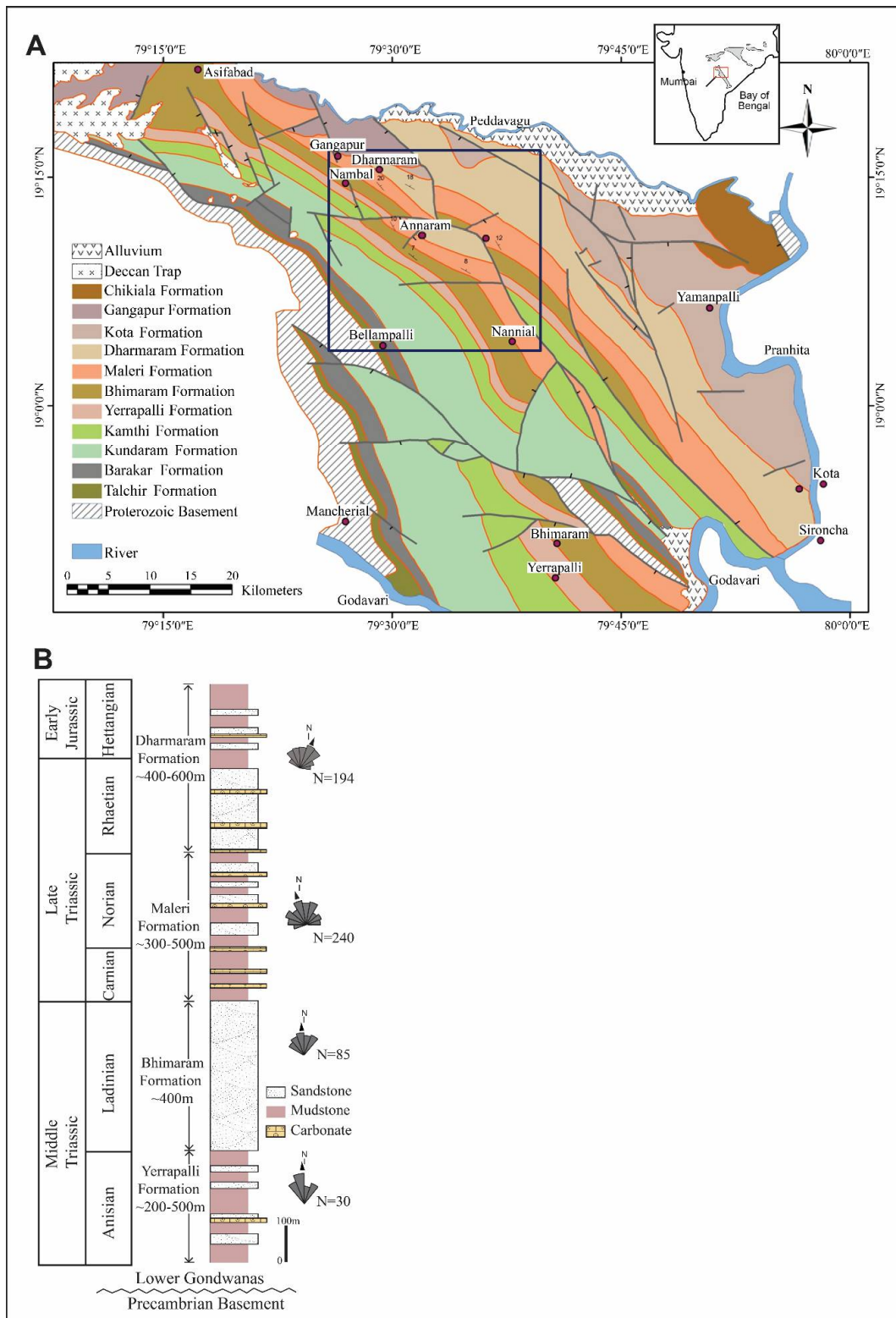


Figure 1. (A) Geological map of northern Pranhita-Godavari syn-rift basin, adapted from [39,50]. The study area is marked by a square. Inset shows the relative positions of the main Gondwana outcrops in the Indian subcontinent; the Pranhita-Godavari basin is marked (position of this map marked in red box). (B) Stratigraphic divisions and composite lithology of the four Mesozoic formations discussed in this study are shown. Paleocurrent data documented for this study, from all the four formations, is supported by earlier research work as well [38–41,51–53].

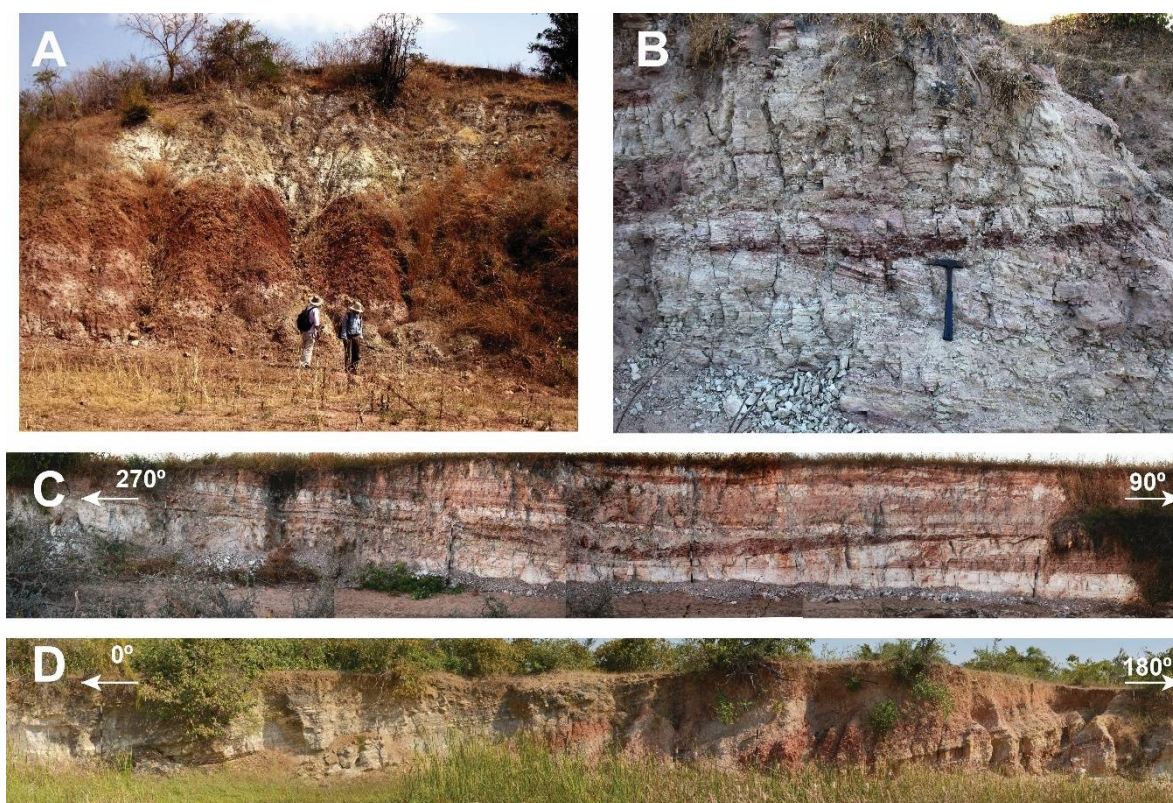


Figure 2. (A) Field photograph showing fine-grained sheet sand body overlying a thicker mudstone unit within the Yerrapalli formation, near Salpalabaigudem village. (B) Field photograph showing medium- to coarse-grained sandstone beds intercalated with minor red mudstone beds near Salpalabaigudem village within the Bhimaram formation (hammer length = 37 cm). (C) Field photograph of Maleri formation showing very-fine- to medium-grained multi-storied sheet sandstone body composed of alternating sandstone and mudstone beds within the Maleri formation near Aklapalli village. (D) Field photograph showing very-coarse- to fine-grained sandstone bodies within the Dharmaram formation alternating with mudstone units, near Paikashigudem village. Scale bar = 1.5 m.

4. Results

A brief facies analysis of mainly the siliciclastics of the four different formations studied here is given in Table 2. These nine different facies occur in different associations in the four formations; however, detailed work is not the focus of this present study.

4.1. Paleocurrent Directions

Planar and trough cross-bedded fine- to coarse-grained sandstone units of Yerrapalli, Bhimaram and Maleri formations show an overall northerly paleocurrent direction (mean values of 359° , 330° and 356° , respectively) (Figure 1B; [29,40,51–53]). The Dharmaram formation exhibits a northeasterly paleocurrent direction (mean value 035°) (Figure 1B).

4.2. Petrography

The sandstone of the Yerrapalli formation is moderately well-sorted arkosic arenites, consisting of quartz and orthoclase feldspar grains, with an average composition of $Q_{55-97}F_{2-45}L_{0-2}$ (Table 3). The framework grains are mostly fine- to medium-grained, sub-angular to sub-rounded, and cemented by calcite (Figure 3A). Monocrystalline grains dominate the quartz fraction. Some of the monocrystalline quartz shows slight to strong undulose extinction. Point contact between the framework grains are observed. Heavy minerals, biotite grains and mud aggregates occur locally (Figure 3B,C).

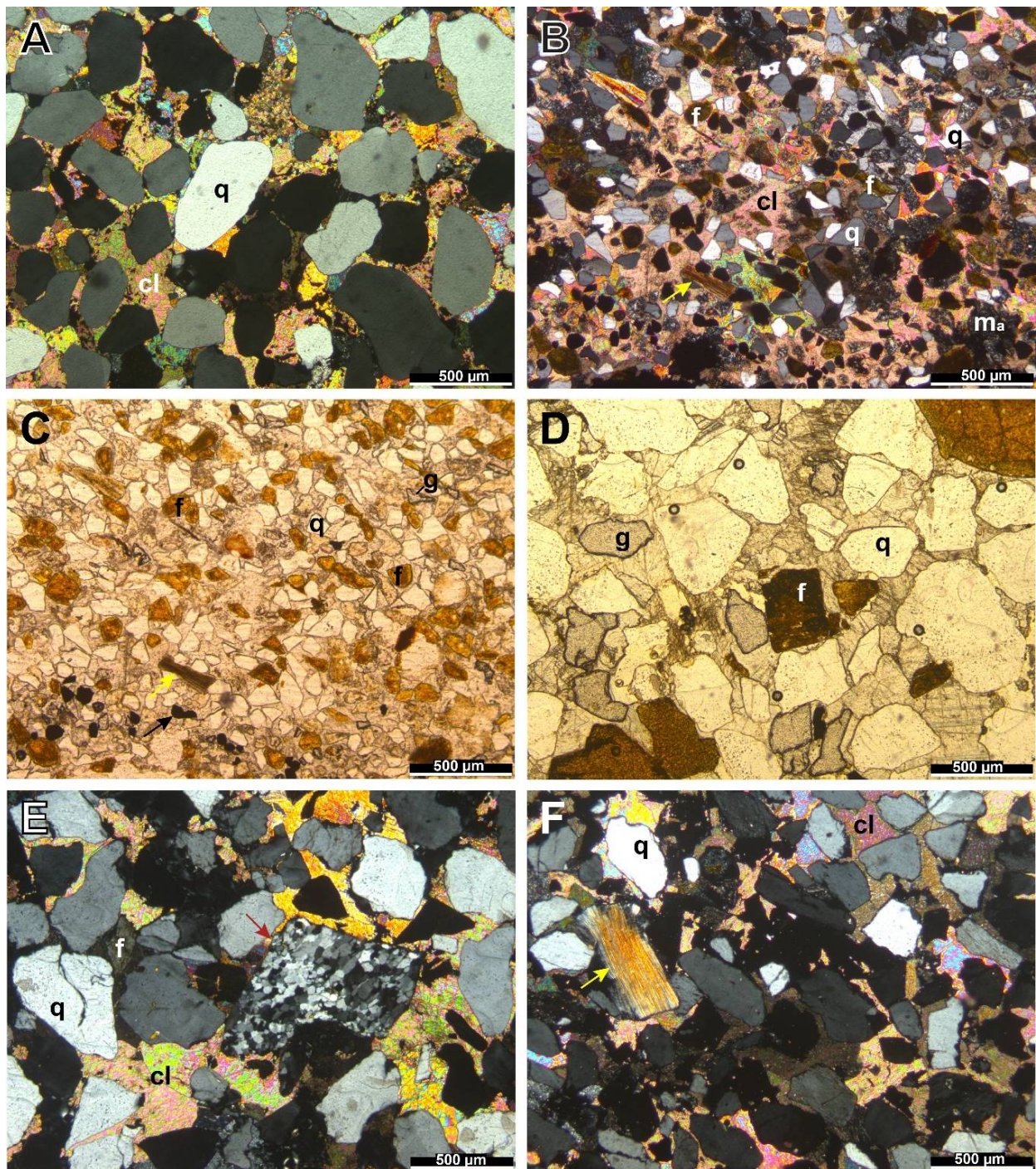


Figure 3. Photomicrographs showing (A) sub-angular to sub-rounded, medium-grains of quartz grains (q) and orthoclase feldspar, floating in poikilotopic calcite cement (cl) as seen under cross-polarized light; (B) fine biotite grains (yellow arrow), stained feldspar grains (f) and mud aggregates (ma) as seen under cross-polarized light; (C) fine grains of stained orthoclase feldspar (f), black opaque minerals (black arrow) and garnets (g) as seen under plane-polarized light, within the Yerrapalli sandstone sample. Photomicrographs showing (D) point contact between the medium-to coarse-sand-size, sub-angular framework grains, stained orthoclase feldspar (f) and garnet (g) in otherwise floating grains in poikilotopic calcite cement as seen under plane-polarized light; (E) lithic fragment (red arrow) and (F) biotite grains (yellow arrow) as seen under cross-polarized light, within the Bhimaram sandstone sample.

The Bhimaram sandstone is moderately sorted subarkosic arenite made up of mainly quartz grains with a few K-feldspars, with a general composition of $Q_{79-84}F_{15-19}L_{1-2}$ (Table 3). The framework grains are mostly medium-grained and sub-angular. Although most quartz grains are monocrystalline, a few polycrystalline grains are also present. Few grains of mica, heavy minerals and lithic fragments are present (Figure 3D–F). Grains show point contacts.

Maleri sandstone is moderately well-sorted fine- to medium-grained arkosic to subarkosic arenite consisting of quartz and orthoclase feldspar, and has a general composition of $Q_{64-97}F_{3-36}L_{0-1}$ (Table 3). Sand-sized mud aggregates, carbonate grains, lithic fragments and heavy and opaque minerals are the subordinate components. The framework grains are subrounded in shape with moderate sphericity. They dominantly show point contact between grains, along with a few sutured and long contacts. Both monocrystalline and polycrystalline quartz grains are present. Some of the monocrystalline quartz shows slight to strong undulose extinction. Only K-feldspar is present. Heavy minerals, micas and opaques comprise a small fraction of the framework constituents. Poikilotopic calcite cement occupies the intergranular spaces (Figure 4A,B).

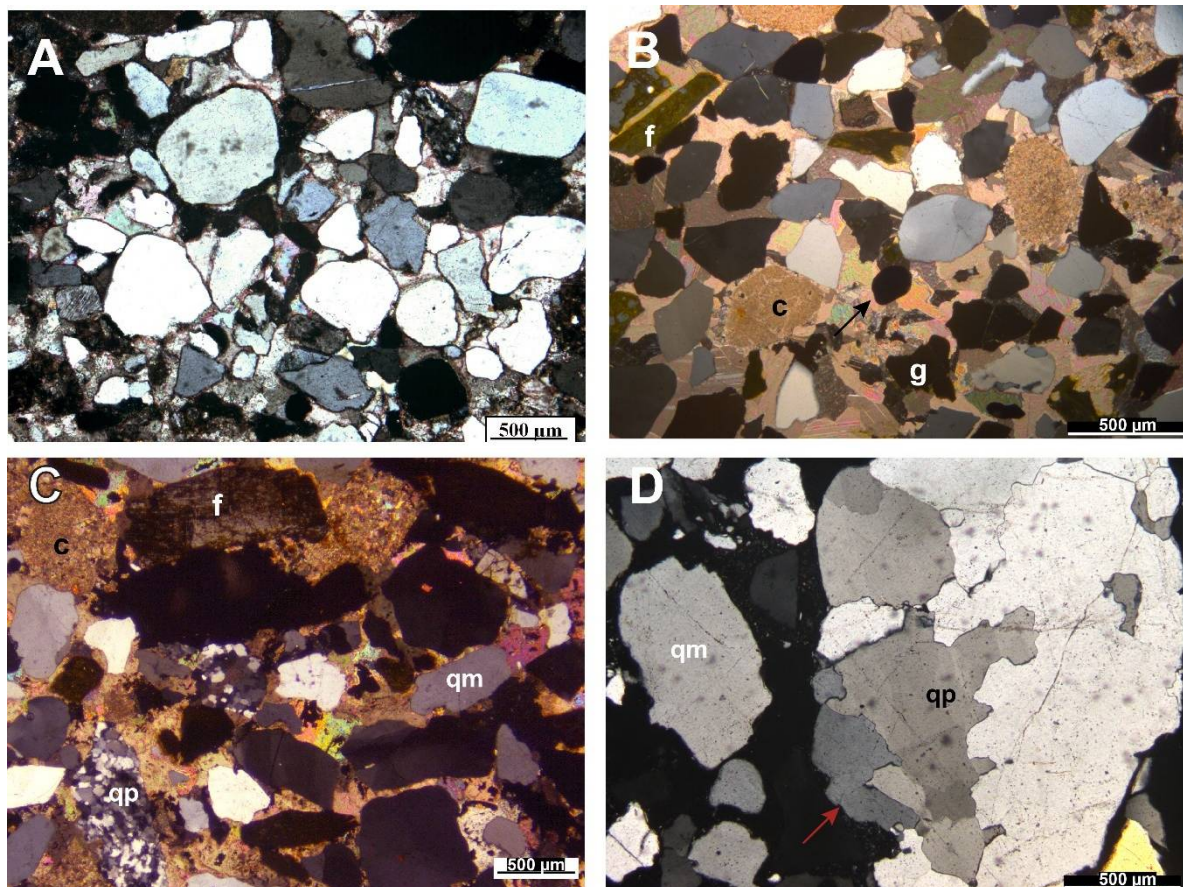


Figure 4. Photomicrographs showing (A) fine- to medium-sand-size, sub-rounded to sub-angular framework grains with dominantly tangential or point contact between them; (B) fine- to medium-sand-size framework grains of carbonate (c) and stained orthoclase feldspar (f) along with a few opaque heavy minerals (black arrow) and garnet (g), with poikilotopic calcite cement occupying the intergranular spaces within the Maleri sandstone sample. Photomicrographs showing (C) mostly quartz (monocrystalline-qm and polycrystalline-qp) and k-feldspar (f) grains along with carbonate grains (c) with tangential or point contact between the framework grains, in poikilotopic calcite cement; (D) medium- to coarse-sand-size, sub-angular polycrystalline quartz grain (red arrow), within the Dharmaram sandstone sample.

Dharmaram sandstone is made of moderately to poorly sorted, mostly quartz and K-feldspar grains. The framework grains show polymodal distribution. A subordinate amount of mica, carbonate grains, lithic fragments and opaque minerals are also present. The occurrence of polycrystalline quartz grains with tectonic fabric is common, unlike other formations studied here. The framework sand is medium to coarse and mostly sub-angular. This sandstone is subarkosic to sublitharenitic, with a general composition of $Q_{63-90}F_{3-36}L_{0-12}$ (Table 3). The quartz is mostly monocrystalline, although the polycrystalline variety is also found. Grains show mostly point contact and are locally sutured with irregular boundaries. Calcite cement dominates the interstitial spaces. (Figure 4C,D).

The Gondwana sediments in the QFR plot (adapted from [55]) mostly cluster in the subarkose area (Figure 5A). In the QmFLt plot (adapted from [56]), sediments of Yerrapalli and Maleri formations mostly cluster in the transitional continental provenance, whereas those of Bhimaram and Dharmaram formations mainly cluster within the cratonic interior field (Figure 5B).

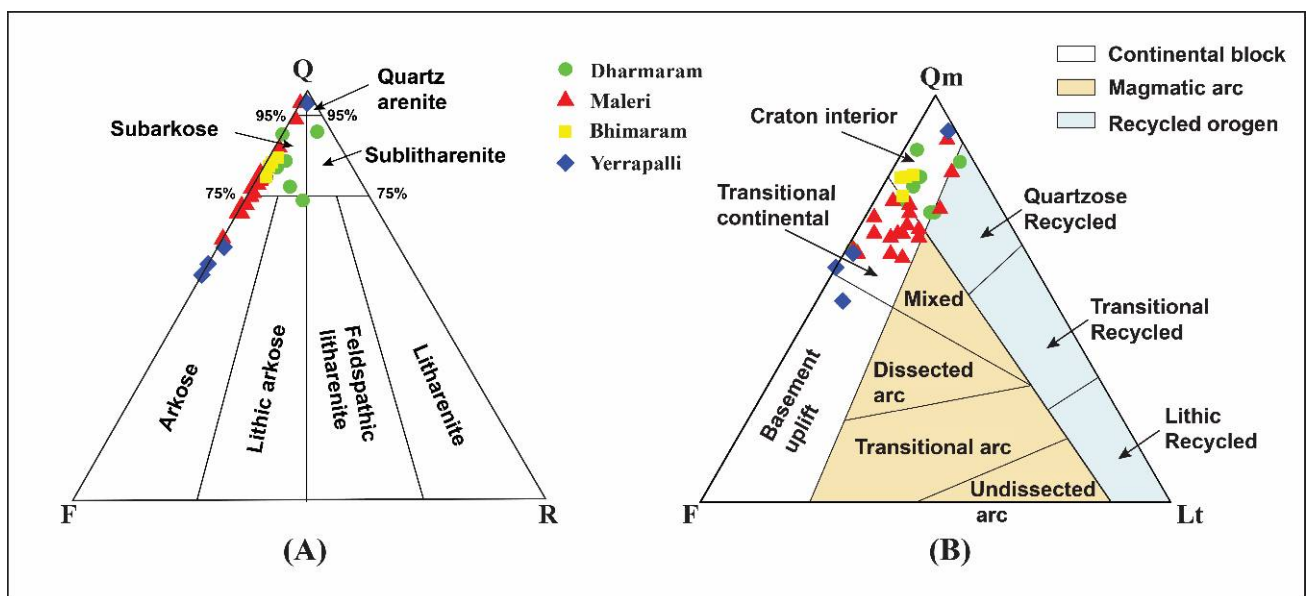


Figure 5. (A) QFR plot (adapted from [55]) and (B) QmFLt plot (adapted from [56]) for sandstone samples of Yerrapalli, Bhimaram, Maleri and Dharmaram formations (Q—total quartzose grains (Qt), including monocrystalline (Qm) and polycrystalline (Qp) varieties, F—total feldspar grains, R—total unstable rock fragments, L—total unstable lithic fragments, Lt—L + Qp).

4.3. Geochemistry

4.3.1. Major Oxides

The SiO_2 content of the mudstone from the Dharmaram and Yerrapalli formations is the highest with 50–70%, with only 50–60% in the Maleri formation. Al_2O_3/TiO_2 varies between 15 and 24, with the highest and lowest values in Yerrapalli and Dharmaram samples, respectively (Table 4). Compared to the PAAS values, the mudstone samples have lower values for SiO_2 (except a few), Al_2O_3 , Na_2O and K_2O , and higher values for Fe_2O_3 and CaO (Figure 6A,B). The contents of MnO and P_2O_5 are very low and display no major differences between the different formations. LOI values range from 7.4 to 15.96 wt% (Table 4). The CIA values of the Mesozoic samples range between 61% and 94% (Table 4). The ICV values of the Mesozoic samples vary from 0.5 to 1.4 (Table 4). The mudstone samples with high CIA have low ICV values and vice versa.

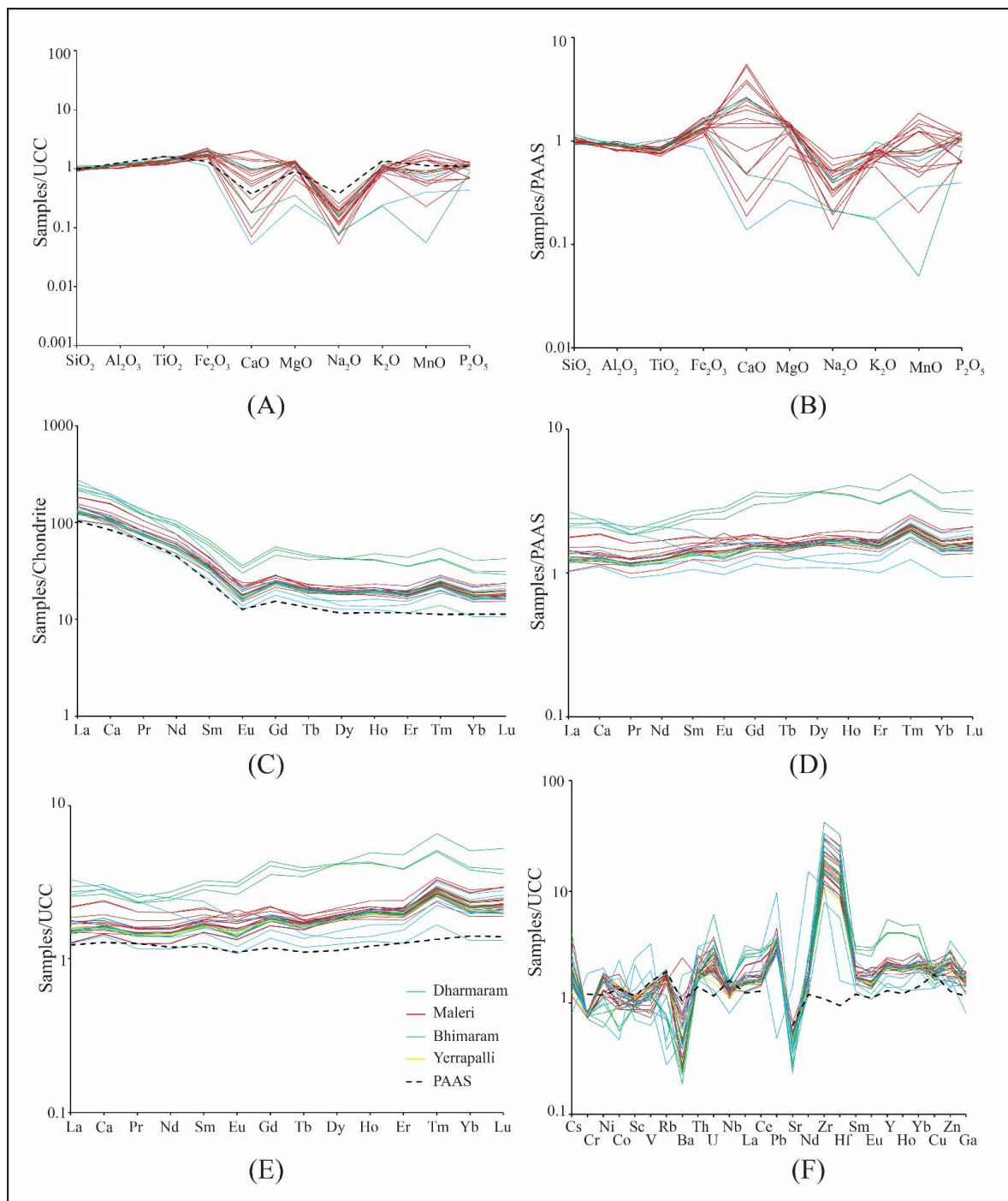


Figure 6. (A) Upper continental crust (UCC, [48])-normalized major element composition. (B) Post-Archean average Australian shale (PAAS, [47])-normalized major element composition. (C) Chondrite-normalized rare earth element (REE) plots for the Gondwana mudstone samples showing generally higher concentrations of light REE (LREE) than heavy REE (HREE), with a negative Eu-anomaly. Chondrite normalization values; REE compositions of PAAS (black dash line) are from [47]. (D) PAAS-normalized REE patterns showing positive values for both LREE and HREE. REE compositions of PAAS are from [47]. (E) UCC-normalized REE patterns showing uniform and positive pattern for both LREE and HREE. REE compositions for UCC are from [48]. (F) Spider plot of trace element compositions normalized against upper continental crust (UCC; [48]) for Gondwana mudstone samples. PAAS values are represented by the black dashed line [47].

4.3.2. Trace Elements

The concentration of Zr decreases from 8000 ppm in the oldest Yerrapalli samples to 1500 ppm for the youngest Dharmaram samples (Table 5). The concentrations of Zr (avg. 3900 ppm; ranging from 1535 ppm to 8036 ppm) and Hf (avg. 80 ppm; ranging from 31 ppm to 170 ppm) in the samples are considerably higher than that of the PAAS (210 ppm and 5 ppm, respectively). Samples of all formations show a higher average concentration of Th (avg. 20.4 ppm) compared to PAAS (14.6 ppm). The Zr/Sc ratio of samples shows considerable variation (135–455), whereas the Th/Sc ratio is primarily consistent (1–2.4) (Table 7) and matches with the values of PAAS and standard shale samples (see Table 2 of [57]). However, the Zr/Sc ratio for the Yerrapalli formation shows a much higher range as compared to the younger formations. Similarly, the Y/Ni ratio of the Yerrapalli formation is much higher (avg. 1.25) as compared to the younger formations (~0.6). The Th/Co ratio is considerably consistent throughout the Mesozoic succession (0.5–2). The Cr/V ratio is also consistent throughout, ranging between 0.2 and 1.

4.3.3. Rare Earth Elements (REE)

Samples of the Yerrapalli formation show higher content of Σ REE (226–449 ppm, Table 7), while those of the Maleri and Dharmaram formations exhibit lower Σ REEs, ranging between 210–327 ppm and 192–392 ppm, respectively (Table 7). The REE concentrations of the Mesozoic mudstone samples are normalized against chondrite, PAAS and UCC (values taken from [47]) (Figure 6C–E). The chondrite-normalized REE patterns of the samples show LREE enrichment, relatively flat HREE, and a low to moderate LREE/HREE ratio (~6–15, Figure 6C; Table 7). UCC-normalized values reveal a more or less uniform positive pattern (Figure 6E). Most chondrite-normalized mudstone samples show a narrow range of Europium anomaly (Eu/Eu*) values lying between 0.5 and 0.8. This range is close to that of PAAS (0.64) (Table 7).

5. Interpretation and Discussion

5.1. Composition of Source Rock

The LREE enrichment and the resemblance of the chondrite-normalized REE patterns to those of PAAS and negative Eu anomalies endorse the dominance of felsic source rocks in sediments [22,23,26,58–62] (Figure 6B). High ratios of Th/Sc and Th/Co indicate felsic sources (Figure 7A,B; Table 7). Cross-plot of Th/Co versus La/Sc, triangular plot of V-Ni-Th $\times 10$ indicate the predominantly felsic provenance (Figure 7B,C). The abundance of zircons in the studied sandstones supports the felsic provenance (Table 5). The low Cr/V and fairly low Y/Ni is in accordance with a mix of granite and ultramafic rocks (Figure 7D) (cf. [57,63,64]). Low La/Th ratios (ranging from 2 to 5) indicate a predominant felsic source of sediments [65–69] (Table 7). Field observations and petrographical study of sandstones in Yerrapalli, Bhimaram, Maleri and Dharmaram formations indicated a predominant felsic source rock (Figure 5A). The geochemical data of mudstone samples corroborate the felsic source of the studied formations.

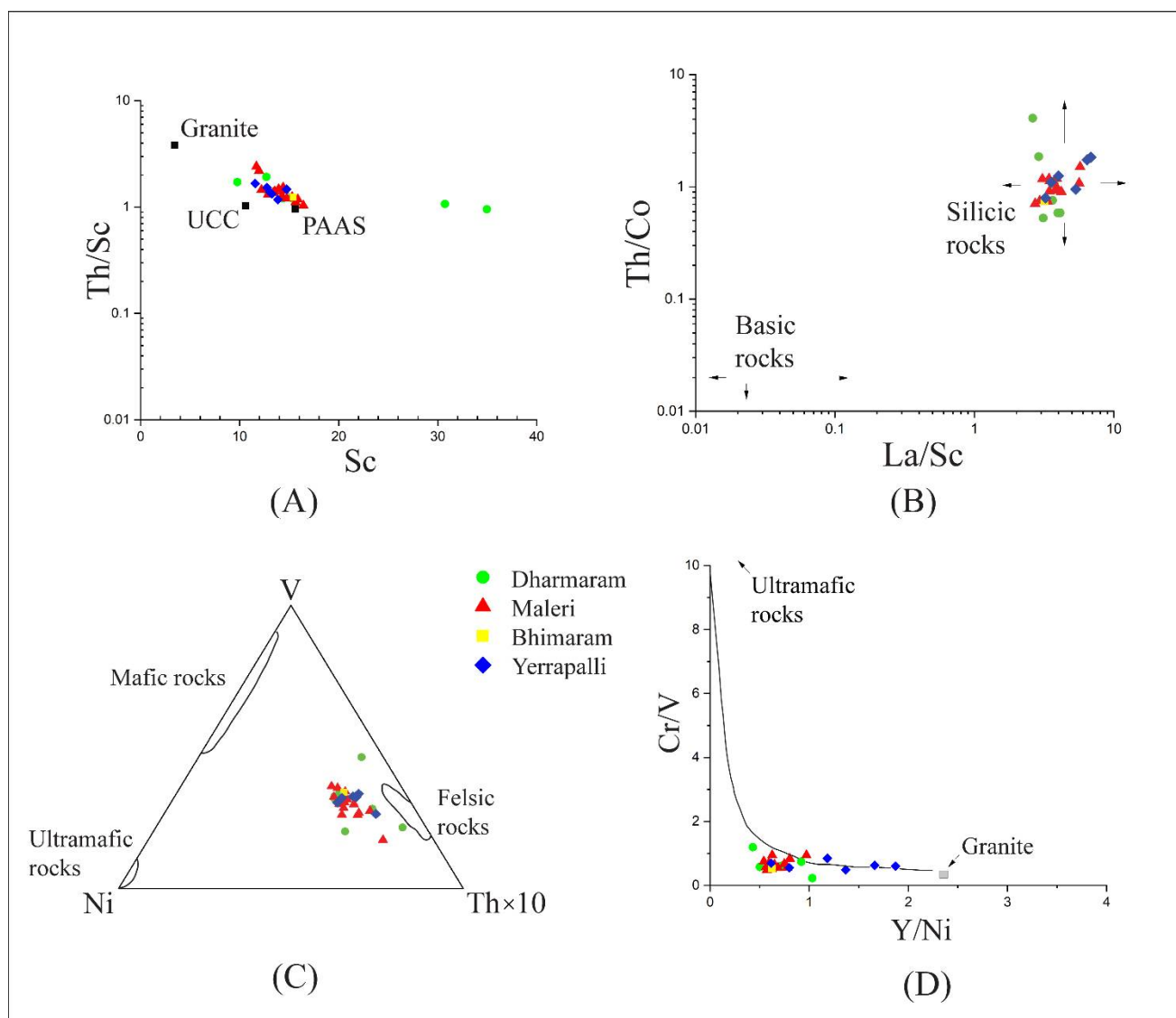


Figure 7. Source rock discrimination based on cross-plots of (A) Th/Sc and Sc (adapted from [70]), (B) Th/Co and La/Sc ratios [71], (C) V-Ni-Th \times 10 plot [72] and (D) Cr/V and Y/Ni (adapted from [73]) for Gondwana mudstone samples.

5.2. Source Area Weathering and Recycling

The combined ICV and CIA values of the mudstone samples indicate intermediate weathering at the time of deposition for most of the samples (Figure 8A,B). The weathering trend observed in Figure 8A indicates depletion of Ca and Na (considering disappearance of plagioclase already), with more K-feldspar, illite and kaolinite in the sediments. The absence of plagioclase in sandstone petrography supports this view. This suggests an advanced stage of weathering, probably due to decreasing input of first cycle detritus coupled with recycling of sedimentary material [54,74]. However, two mudstone samples show a more mature source with higher CIA values, which could be due to compositional variation in the sediment itself. Recycling of sediments is indicated by the high Th/Sc and Zr/Sc [75] (Figure 8C; Table 7). Zr/Sc ratios increase almost independently of Th/Sc ratios due to the high concentration of the heavy mineral zircon (Table 5). The petrographic observations also reveal mostly medium-fine sub-rounded grains of the older formations and comparatively coarser sub-angular of the Dharmaram formation, suggesting more transportation of the older sediments.

5.3. Tectonic Setting

The measured paleocurrent data during Gondwana sedimentation, as documented for this study, are consistent with those obtained by previous workers [38–41,51–53] (Figure 1B). The N-NW paleocurrent direction suggests the transportation of most detritus from the highs located in the south and southeasterly direction. Though an axial drainage system was dominant, small transverse drainages also persisted along the fault margins during the Mesozoic era [53]. However, north-easterly paleocurrent data of the youngest Dharmaram formation indicate the reversal in the direction of sediment supply. As the Gondwana breakup had started since the Jurassic time [1–4,29], this shift in the paleocurrent data suggest a change in paleoslope. The sub-angular framework grains with polymodal distribution of Dharmaram sandstones, along with increased lithic fragments, might point to an elevated western basinal margin. The high content of quartz and feldspar is typical for sand related to transitional continental (Yerrapalli and Maleri formations) to craton interior provenance (Bhimaram and Dharmaram formations) (Figure 5B). Less significant variation in climate-sensitive proxies corroborates the continuation of syn-rift tectonic setting within the Pranhita-Godavari Gondwana basin (Figure 9; Tables 5 and 7). In the cross-plot of Eu/Eu^* and (Gd_N/Yb_N) , the majority of Yerrapalli, Bhimaram, Maleri and Dharmaram mudstone plots in the field of post-Archean rocks indicate a dominance of the post-Archean source (Figure 10A). Further, the lower values in the Cr vs. Ni cross-plot corroborate the post-Archean age of the source (Figure 10B, [47]). The positive $(La/Yb)_N$ values (ranging between 5 and 14, ~avg. 8.23) and $(La/Sm)_N$ values (ranging between 3 and 8, ~avg. 4.09) of the studied samples indicate an early diagenesis adsorption mechanism [76]. Since all the fossils documented in the studied formations are continental, along with the sedimentological and geochemical evidence, deposition took place in a fluvial, intracratonic setting.

Schematic block diagrams showing the organization of the Middle Triassic–Early Jurassic paleogeography is given in Figure 11. Please refer to Table 2 of [52] for the details of the Pranhita-Godavari Proterozoic rocks lying on either side of the Pranhita-Godavari Gondwana basin deposit. The Khammam Schist belt and the Eastern Ghat and Karimnagar Granulite belts surround the Proterozoic sedimentary rocks [31]. Age dating of the zircon and monazite heavy minerals of the basin-fill Gondwana rocks and correlating them with those from the hinterland in the surroundings will be a direct provenance study in the future. A future work taking into consideration the isotope compositions of Strontium (Sr), Niobium (Nb), and Rubidium (Rb) can be performed for further understanding the palaeoclimate and for paleogeographic reconstructions. Pearson's r correlations and discriminant function multi-dimensional plots remain to be analyzed for better understanding and interpretation of the tectonic setting [77–79]. A provenance study of the remaining formations of Pranhita-Godavari Gondwana basin, lying above Dharmaram formation, needs to be conducted in the future. It is noteworthy that due to the reversal of the drainage pattern post-Madagascar rifting, the paleocurrent should record a change in direction from the Late Cretaceous [37]. Hence, a change of source is expected thereafter.

5.4. Paleoenvironmental Implication

The presence of gypsum crystals in the mudstones of the Yerrapalli formation indicates precipitation of sulphate in a water-logged condition corresponding to a semi-arid environment. Essentially, the environment was fluvatile, with seasonal to semi-arid climatic condition. Scarce vegetation in the Yerrapalli formation indicates that the considerably low water table and prevailing oxidizing condition were not suitable for the preservation of plant life [51].

The sub-mature nature, coarser grain size and loosely packed grains of the Bhimaram formation suggest that these sandstones were deposited in a fluvial environment with high velocity. The coarse argillaceous sandstones produced bar complexes such that the sediments of the channel and the inter-channel facies amalgamated together to form a

thick sandstone body (Table 2). Essentially, the climate was moist enough for the growth of vegetation.

The petrographic and geochemical studies of the sediments and extensive aquatic fossil record of the Maleri formation suggests that the climate was semi-humid to humid during the Late Triassic. The high abundance of mud aggregates along with shrink and swell clay rich sediments suggests a seasonal climatic condition [52]. The fact that all the stable isotope data of the Maleri carbonate samples are comparable to those of the Quaternary tufa sediments [40] suggests that the temperature during deposition of the Maleri sediments was comparatively cooler.

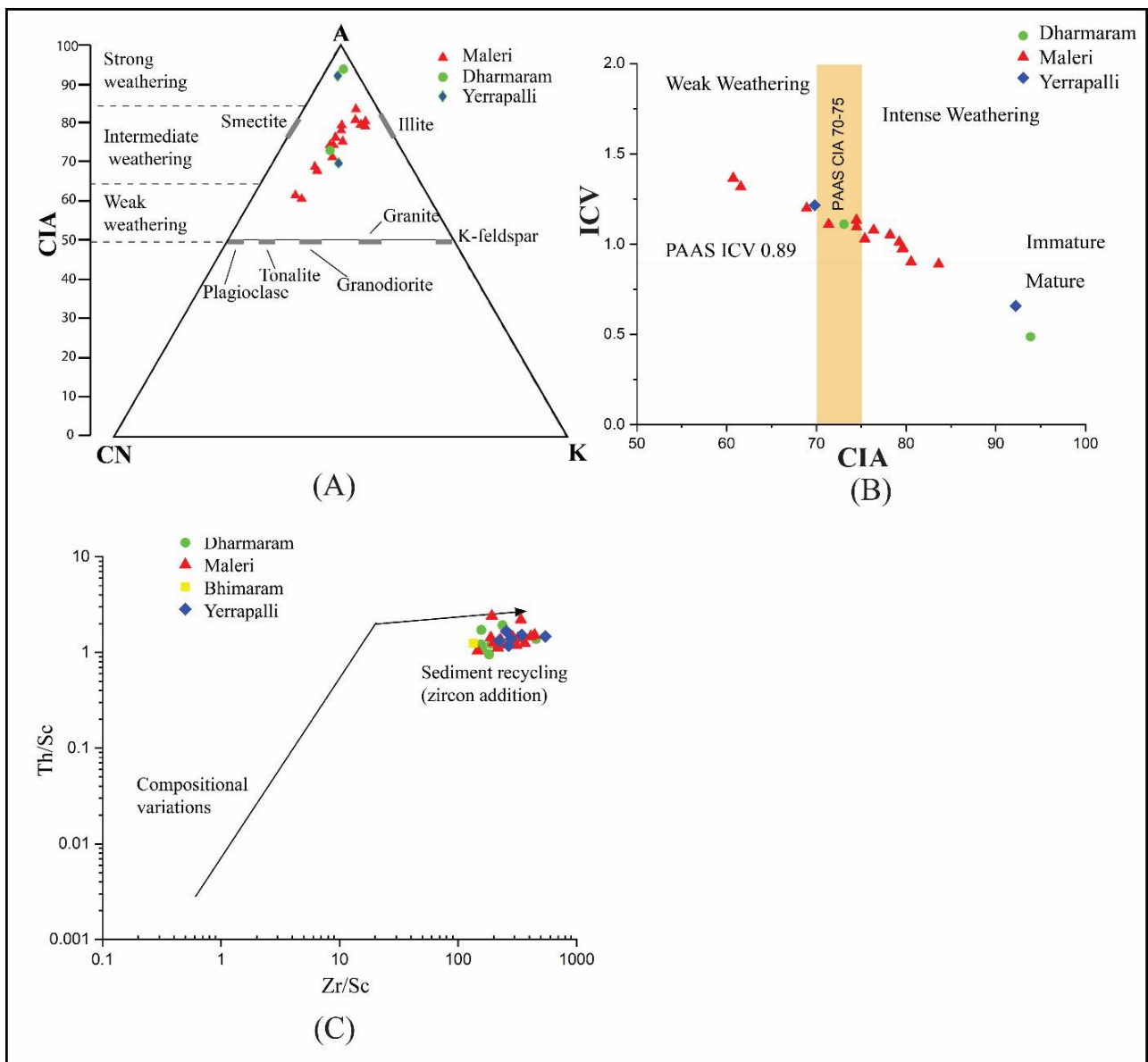


Figure 8. (A) Major element composition plot in an A-CN-K [74] diagram indicating the extent of weathering for the mudstone samples of the Yerrapalli, Maleri and Dharmaram formations. (B) CIA versus ICV. indicating maturity and intensity of weathering (adapted from [80]) for the mudstone samples of Yerrapalli, Maleri and Dharmaram formations. (C) Th/Sc versus Zr/Sc plot of the Gondwana mudstone samples showing enrichment of zircon (high Zr/Sc ratio), indicating derivation of sediment recycling [75].

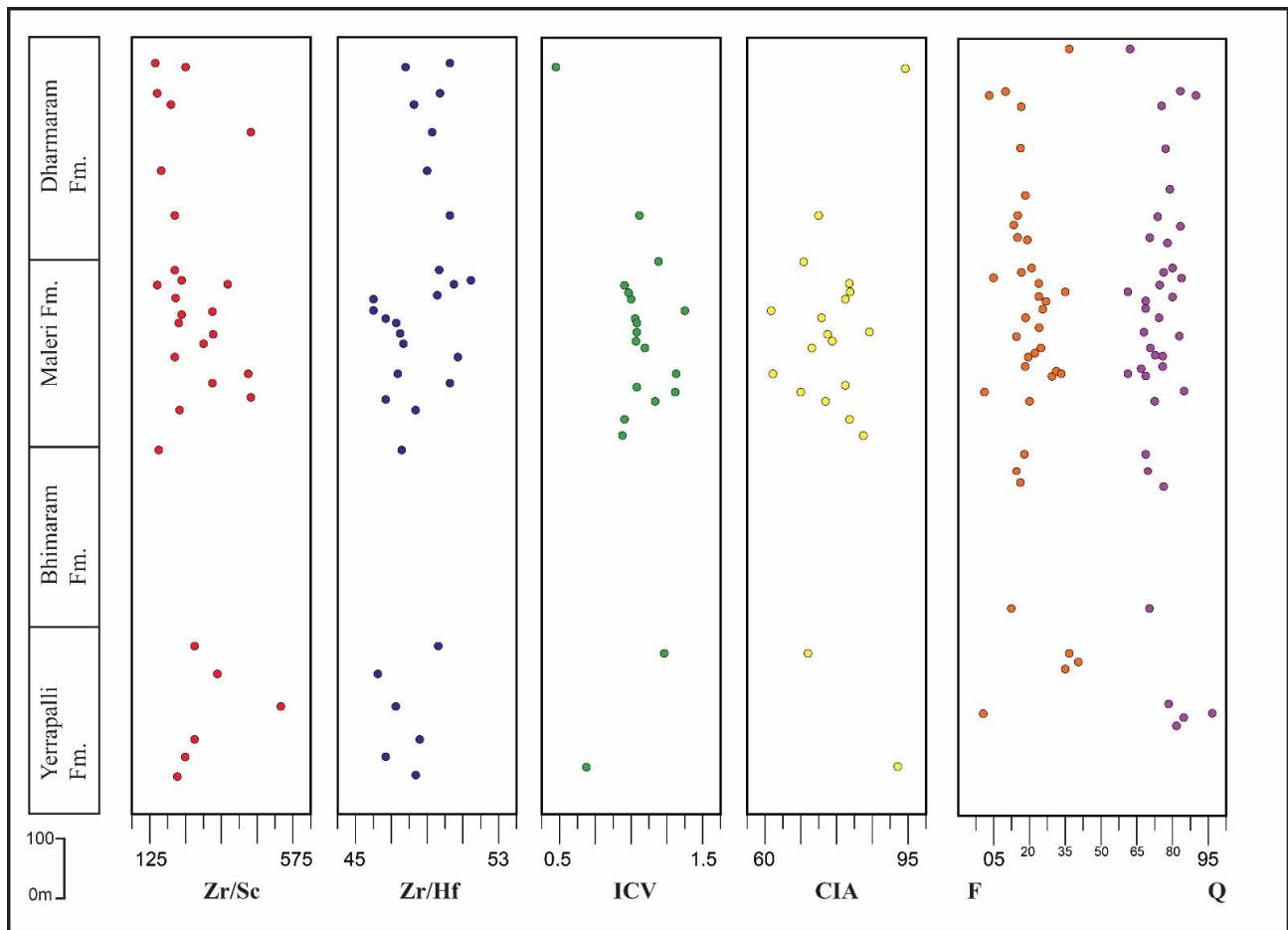


Figure 9. Variations of climate-sensitive proxies (Zr/Sc, Zr/Hf, ICV, CIA) across the Mesozoic formations of the Pranhita-Godavari Gondwana basin. The Zr/Sc content of the mudstones show a broadly similar trend despite minor variation, whereas Zr/Hf content shows a slight increasing trend from older to younger formations. Note that the mudstone samples with high CIA have low ICV (Orange for F and purple for Q in the last figure).

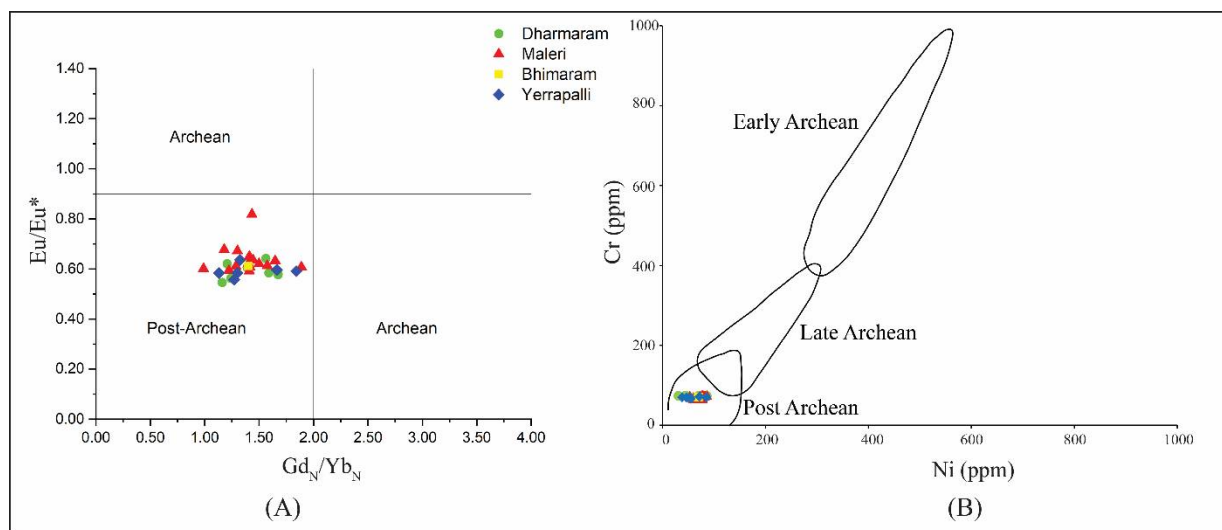


Figure 10. (A) Plot of Eu/Eu* versus (Gd_N/Yb_N) [81] and (B) plot of Cr versus Ni [47] for mudstone samples of the Yerrapalli, Bhimaram, Maleri and Dharmaram formations.

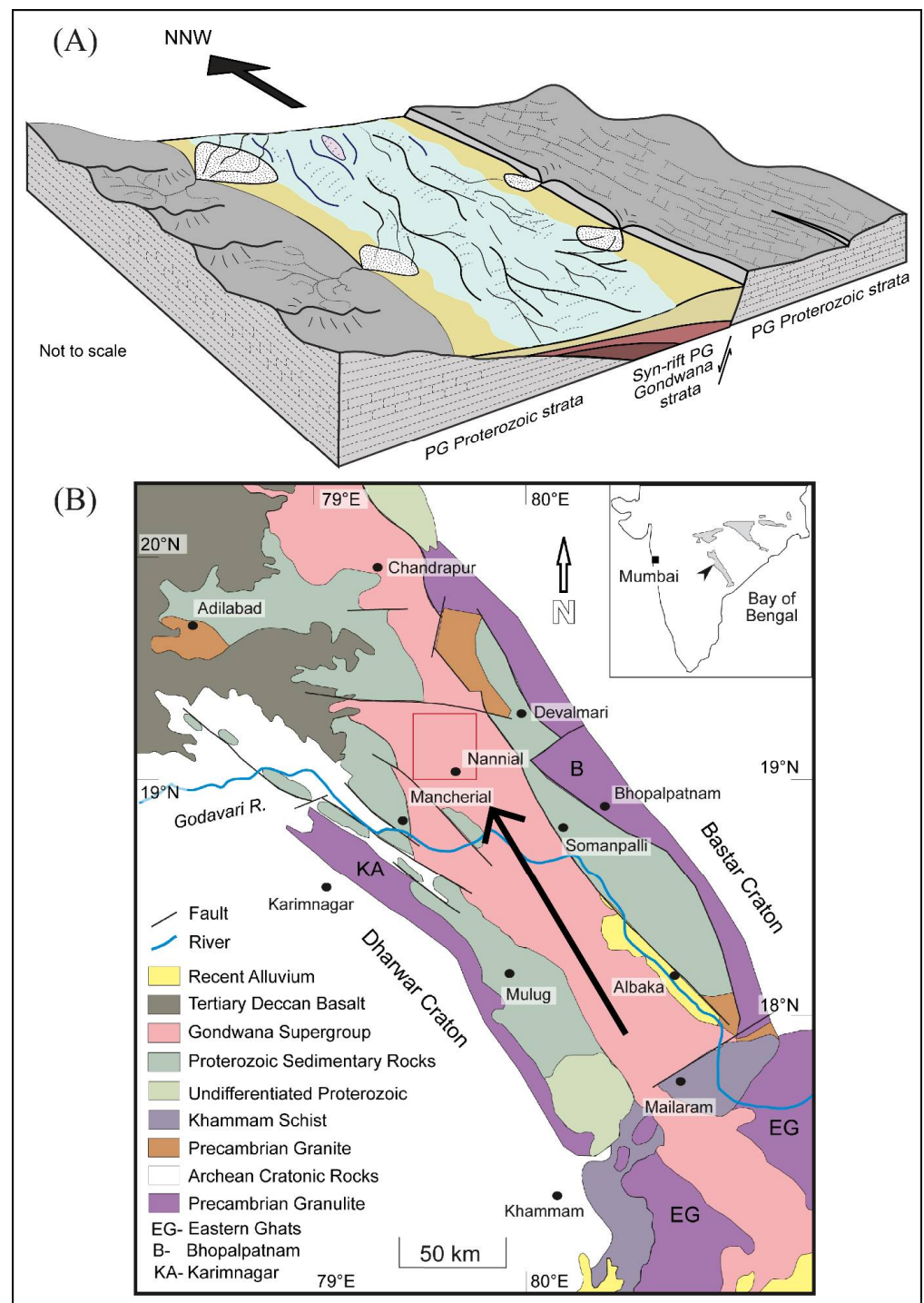


Figure 11. (A) Schematic diagram showing the Middle Triassic–Early Jurassic paleogeography of the Pranhita-Godavari (PG) Gondwana basin, indicating the dominance of the axial drainage system (arrow), along with a few transverse drainages (locally occurring along alluvial fans) on either side that persisted during the Mesozoic era. (B) Black arrow indicates the inferred paleoslope (parallel to the axial drainage system shown in ‘A’) in the geological map showing the exposure belt of the Gondwana supergroup of the Pranhita-Godavari rift basin, India, flanked on either side by the Precambrian rocks (adapted from [31]). The paleocurrent direction indicates most of the detritus were transported from the highs located in the S-SE direction with respect to the Gondwana basin along the axial drainage system. The study area is marked by a rectangle, which corroborates with the study area shown in Figure 1A.

The presence of immature sandstone along with the easterly dipping palaeocurrent direction of the Dharmaram sediments suggests a less reworked, less matured local provenance, mainly from the western margin of the rift basin. This also explains the occurrence of thicker and coarser sandstone bodies. The presence of poikilotopic calcite cement in association with shell fragments of aquatic organisms and presence of large petrified wood fragments confirms a wetland condition that prevailed during sedimentation of the Dharmaram formation. Thus, the climate was more humid during the Early Jurassic.

Hence, it can be said that there was a gradual change with respect to tectonism and climatic condition, as well as the nature of sedimentation, from the early Middle Triassic to the early Early Jurassic period in the Pranhita-Godavari rift basin. Schematic block diagrams showing the organization of the paleoenvironments during the above-mentioned time interval are given in Figure 12. Although a brief facies analysis has been given in Table 2, a thorough study of sedimentological details remains to be conducted for the Yerrapalli, Bhimaram and Dharmaram formations, in order to elaborate on the paleoenvironmental conditions.

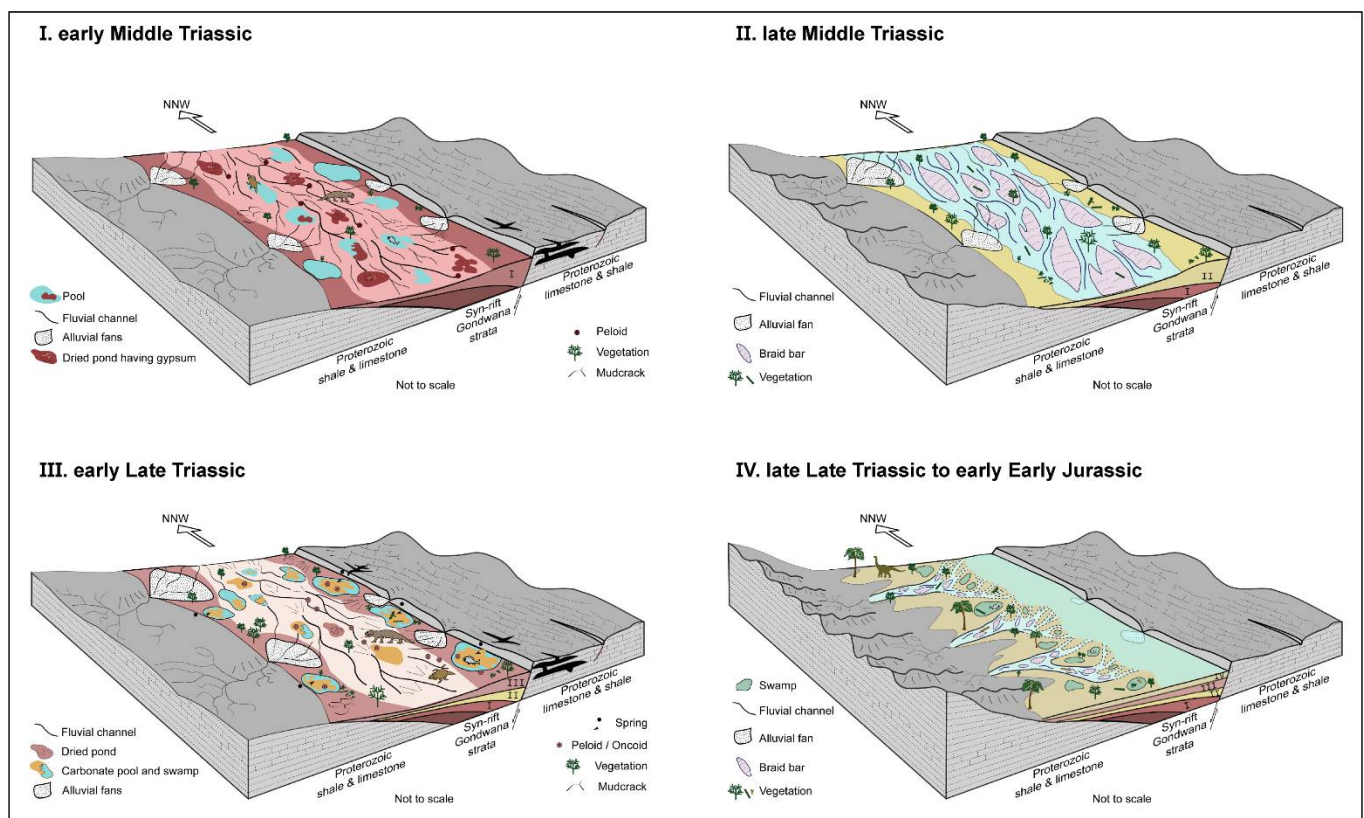


Figure 12. Schematic block diagrams representing the organization of the palaeoenvironments in the Pranhita-Godavari Gondwana rift-basin flanked by Proterozoic sedimentary rocks is shown. (I) shows the spatial relationship among different types of lithology during the early Middle Triassic, when fine sediments of the Yerrapalli formation were deposited; (II) shows the scenario of the late Middle Triassic, when essentially sandstone deposition took place during the sedimentation process of the Bhimaram formation; (III) shows the setting of the early Late Triassic sediments of the Maleri formation [40,52]; (IV) shows the scenario of the late latest part of the Triassic to early Early Jurassic when the coarse sediments of the Dharmaram formation were deposited in a transverse system, unlike in the previous stages, during which sediments were deposited in the axial drainage system. Note that the large waterbody in figure (IV) represents the lacustrine environment of the overlying Lower Kota formation [82,83], the details of which are not the focus of this paper.

6. Conclusions

This study presents the first comprehensive mineralogical-geochemical investigation of early Middle Triassic to early Early Jurassic sediments of the Pranhita-Godavari syn-rift Gondwana basin of peninsular India. Geochemical compositions of the mudstones and petrography of sandstones were analyzed to identify provenance, paleoweathering conditions and tectonic setting. The geochemical data of major and trace elements show that the studied rocks have the same source. The QFR and QmFLt plots indicate the derivation of sediments from cratonic interior and transitional continental origin. Sandstone shows a gradual shift from arkose to subarkose in the Yerrapalli, Barakar and Maleri formations, and to sublithic arenite sandstones in the younger Dharmaram formation. Trace element data suggests the predominance of post-Archean source rocks. The chemical composition of Mesozoic mudstone samples reveals intermediate weathering conditions from Early Middle (Yerrapalli formation) to early Early Jurassic (Dharmaram formation). The binary diagrams and source rock discrimination plots reveal that the mudstones are mostly of felsic provenance. A change in tectonism and sediment supply is suggested due to the shift in the paleocurrent direction from NNW to NE, along with a gradual change in paleoclimate from semi-arid to humid condition, which is corroborated by petrographical observation as well. This shift might suggest the initiation of paleoslope reversal. The provenance, along with the paleocurrent data during Middle Triassic–Early Jurassic, indicate that the source might have been adjacent Proterozoic sedimentary rocks, the Karimnagar Granulite belt, the Khammam schist belt and the Eastern Ghats Granulite belt.

Author Contributions: Conceptualization, S.D. and S.B.; methodology, S.D., S.B. and P.G.; validation, S.D., S.B. and P.G.; formal analysis, S.D.; investigation, S.D. and S.B.; resources, S.B. and P.G.; data curation, S.D. and S.B.; writing—original draft preparation, S.D.; writing—review and editing, S.D. and S.B.; supervision, S.B.; project administration, S.B.; funding acquisition, S.B. and P.G. All authors have read and agreed to the published version of the manuscript.

Funding: This research was developed at the Indian Institute of Technology, Bombay, India, funded by IIT Bombay and Indian Statistical Institute, Kolkata, India.

Informed Consent Statement: Not Applicable.

Data Availability Statement: Not Applicable.

Acknowledgments: The authors are grateful to the Indian Institute of Technology, Bombay and to the Indian Statistical Institute, Kolkata, for providing the financial and infrastructural support for this research. The authors remain thankful to the large number of people who helped in field data collection and laboratory analysis of the samples.

Conflicts of Interest: The authors declare no conflict of interest.

References

1. Reeves, C.; Wit, M. Making ends meet in Gondwana: Retracing the transforms of the Indian Ocean and reconnecting continental Shear Zones. *Terra Nova* **2000**, *12*, 272–280. [[CrossRef](#)]
2. Chatterjee, S.; Goswami, A.; Scotese, C.R. The longest voyage: Tectonic, magmatic, and paleoclimatic evolution of the Indian plate during its northward flight from Gondwana to Asia. *Gondwana Res.* **2013**, *23*, 238–267. [[CrossRef](#)]
3. Dasgupta, S.; Biswas, M.; Mukherjee, S.; Chatterjee, R. Structural evolution and sediment depositional system along the transform margin- Palar–Pennar basin, Indian east coast. *J. Pet. Sci. Eng.* **2022**, *211*, 110155. [[CrossRef](#)]
4. Dasgupta, S. Implication of transfer zones in rift fault propagation: Example from Cauvery basin, Indian east coast. In *Tectonics and Structural Geology: Indian Context*; Mukherjee, S., Ed.; Springer Geology: Cham, Switzerland, 2019. [[CrossRef](#)]
5. Fox, C.S. Coal in India II: The Gondwana system and related formations. *Mem. Geol. Surv. India* **1931**, *58*, 1–241.
6. Robinson, P.L. *The Indian Gondwana Formations—a review. 1st International Symposium on Gondwana Stratigraphy*; International Union of Geological Sciences: Paris, France, 1967; pp. 201–268.
7. Venkatachala, B.S.; Maheswari, H.K. Indian Gondwana-redefined. In *7th International Gondwana Symposium, Sao Paulo, BSIPB*; University of Lucknow: Lucknow, India, 1988; pp. 539–547.
8. Veevers, J.J.; Tewari, R.C. Gondwana master basin of Peninsular India between Tethys and the interior of the Gondwanaland province of Pangea: Geological Society of America. *Memoir* **1995**, *187*, 72.

9. Chakraborty, C.; Nibir, M.; Ghosh, K. Kinematics of the Gondwana basins of peninsular India. *Tectonophysics* **2003**, *377*, 299–324. [[CrossRef](#)]
10. Sarkar, A.; Yoshioka, H.; Ebihara, M.; Naraoka, H. Geochemical and organic carbon isotope studies across the continental Permo-Triassic boundary of Raniganj Basin, eastern India. *Palaeogeogr. Palaeoclimatol. Palaeoecol.* **2003**, *191*, 1–14. [[CrossRef](#)]
11. Mukhopadhyay, G.; Mukhopadhyay, S.K.; Roychowdhury, M.; Parui, P.K. Stratigraphic correlation between different Gondwana Basins of India. *J. Geol. Soc. India* **2010**, *76*, 251–266. [[CrossRef](#)]
12. Ghosh, S.; Sarkar, S.; Ghosh, P. Petrography and major element geochemistry of the Permo-Triassic sandstones, central India: Implication for provenance in an intracratonic pull-apart Basin. *J. Asian Earth Sci.* **2012**, *43*, 207–240. [[CrossRef](#)]
13. Dickinson, W.R. Interpreting detrital modes of graywacke and arkose. *J. Sediment Pet.* **1970**, *40*, 695–707.
14. Dickinson, W.R. Interpreting provenance relations from detrital modes of sandstones. In *Provenance of Arenites*; Zuffa, G.G., Ed.; Reidel: Dordrecht, The Netherlands, 1985; pp. 333–361.
15. Basu, A. Influence of climate and relief on composition of sands released at source areas. In *Provenance of Arenites*; Zuffa, G.G., Ed.; Reidel: Dordrecht, The Netherlands, 1985; pp. 1–18.
16. Pettijohn, F.J.; Potter, P.E.; Siever, R. *Sand and Sandstones*, 2nd ed.; Springer-Verlag: New York, NY, USA, 1987; p. 553.
17. Garzanti, E.; He, J.; Barbarano, M.; Resentini, A.; Li, C.; Yang, L.; Yang, S.; Wang, H. Provenance versus weathering control on sediment composition in tropical monsoonal climate (South China)—2. Sand petrology and heavy minerals. *Chem. Geol.* **2021**, *564*, 119997. [[CrossRef](#)]
18. Dickinson, W.R.; Suczek, C.A. Plate tectonics and sandstone compositions. *AAPG Bull.* **1979**, *63*, 2164–2182.
19. Arribas, J.; Critelli, S.; Le Pera, E.; Tortosa, A. Composition of modern stream sand derived from a mixture of sedimentary and metamorphic source rocks (Henares River, central Spain). *Sediment. Geol.* **2000**, *133*, 27–48. [[CrossRef](#)]
20. Le Pera, E.; Arribas, J.; Critelli, S.; Tortosa, A. The effects of source rocks and chemical weathering on the petrogenesis of siliciclastic sand from the Neto River (Calabria, Italy): Implications for provenance studies. *Sedimentology* **2001**, *48*, 357–378. [[CrossRef](#)]
21. Critelli, S. Provenance of Mesozoic to Cenozoic Circum-Mediterranean sandstones in relation to tectonic setting. *Earth Sci. Rev.* **2018**, *185*, 624–648. [[CrossRef](#)]
22. Armstrong-Altrin, J.S.; Lee, Y.I.; Kasper Zubillaga, J.J.; Trejo Ramirez, E. Mineralogy and geochemistry of sands along the Manzanillo and El Carrizal beach areas, southern Mexico: Implications for palaeoweathering, provenance and tectonic setting. *Geol. J.* **2017**, *52*, 559–582. [[CrossRef](#)]
23. Critelli, S.; Muto, F.; Perri, F.; Tripodi, V. Interpreting provenance relations from sandstone detrital modes, southern Italy Foreland Region: Stratigraphic record of the Miocene tectonic evolution. *Mar. Pet. Geol.* **2017**, *87*, 47–59. [[CrossRef](#)]
24. Quinby-Hunt, M.S.; Wilde, P. The provenance of low-calcic black shales. *Miner. Depos.* **1991**, *26*, 113–121. [[CrossRef](#)]
25. Ochoa, M.; Arribas, M.E.; Arribas, J.; Mas, R. Significance of geochemical signatures of provenance in intracratonic rift basins: Examples from the Iberian plate, Sedimentary provenance and petrogenesis: Perspectives from petrography and geochemistry. *Geol. Soc. Am Bull Spec. Pap.* **2007**, *420*, 99–219.
26. Paikaray, S.; Banerjee, S.; Mukherji, S. Geochemistry of shales from the Paleoproterozoic to Neoproterozoic Vindhyan Supergroup: Implications on provenance, tectonics and paleoweathering. *J. Asian Earth Sci.* **2008**, *32*, 34–48. [[CrossRef](#)]
27. Mondal, M.E.A.; Wani, H.; Mondal, B. Geochemical signature of provenance, tectonics and chemical weathering in the Quaternary flood plain sediments of the Hindon River, Gangetic plain, India. *Tectonophysics* **2012**, *566*, 87–94. [[CrossRef](#)]
28. Garzanti, E.; Resentini, A. Provenance control on chemical indices of weathering (Taiwan river sands). *Sed. Geol.* **2016**, *336*, 81–95. [[CrossRef](#)]
29. Dasgupta, S. A review of stratigraphy, depositional setting and paleoclimate of the different Mesozoic basins of India. In *Mesozoic Stratigraphy of India*; Springer: Cham, Switzerland, 2021; pp. 1–37.
30. Suess, E. *Das Saltilitz der Ende*; Wien: Leipzig, Vienna, 1885.
31. Chaudhuri, A.K.; Deb, G.K.; Patranabis-Deb, S.; Sarkar, S. Paleogeographic and tectonic evolution of the Pranhita-Godavari valley, central India: A stratigraphic perspective. *Am. J. Sci.* **2012**, *312*, 766–815. [[CrossRef](#)]
32. Biswas, S.K. Regional tectonic framework of the Pranhita-Godavari basin, India. *J. Asian Earth Sci.* **2003**, *21*, 543–555. [[CrossRef](#)]
33. Dasgupta, U.; Jain, A.D. A surface geochemical survey over part of the Pranhita-Godavari basin and its impact on the hydrocarbon prospects of the basin. *J. Geol. Soc. India* **2007**, *70*, 187–193.
34. Chaudhuri, A.K.; Deb, G.K.; Patranabis-Deb, S. Conflicts in stratigraphic classification of the Puranas of the Pranhita-Godavari Valley: Review recommendations and status of the ‘Penganga’ sequence. In *Precambrian Basins of India: Stratigraphic and Tectonic Context*; Mazumder, R., Eriksson, P.G., Eds.; Geological Society of London, Memoir: Bath, UK, 2015; Volume 43, pp. 165–183.
35. Krishnan, M.S. *The Geology of India and Burma*; Higginbothams (Pvt.) Ltd.: Madras, India, 1968; p. 536.
36. Goodwin, A.M. *Precambrian Geology: The Dynamic Evolution of The Continental Crust*; Academic Press: London, UK, 1991; p. 666.
37. Gombos, A.M., Jr.; Powell, W.G.; Norton, I.O. The tectonic evolution of western India and its impact on hydrocarbon occurrences: An overview. *Sediment. Geol.* **1995**, *96*, 119–129. [[CrossRef](#)]
38. Sengupta, S. Gondwana sedimentation around Bheemaram (Bhimaram), Pranhita-Godavari Valley, India. *J. Sediment. Petrol.* **1970**, *40*, 140–170. [[CrossRef](#)]
39. Kutty, T.S.; Sengupta, D.P. The Late Triassic Formations of the Pranhita-Godavari valley and their vertebrate faunal succession—A Reappraisal Indian. *J. Earth Sci.* **1989**, *16*, 189–206.

40. Dasgupta, S.; Ghosh, P. Freshwater carbonates within a Late Triassic siliciclastic fluvial system in a Gondwana rift basin: The Maleri Formation, India. *Sediment. Geol.* **2018**, *373*, 254–271. [[CrossRef](#)]
41. Bandyopadhyay, S.; Gillette, D.D.; Ray, S.; Sengupta, D. Osteology of Barapasaurus Tagorie (Dinosauria: Sauropoda) from the early Jurassic of India. *Palaeontology* **2010**, *53*, 533–569. [[CrossRef](#)]
42. Ingersoll, R.V.; Bullard, T.F.; Ford, R.L.; Grimm, J.P.; Pickle, J.D.; Sares, S.W. The effect of grain size on detrital modes: A test of the Gazzi-Dickinson point counting method. *J. Sediment Petrol.* **1984**, *54*, 0103–0116.
43. Bailey, E.H.; Stevens, R.E. Selective staining of K-feldspar and plagioclase on rock slabs and thin sections. *Am. Miner.* **1960**, *45*, 1020–1025.
44. Augustsson, C. Influencing Factors on Petrography Interpretations in Provenance Research—A Case-Study Review. *Geosciences* **2021**, *11*, 205. [[CrossRef](#)]
45. Norrish, K.; Hutton, J.T. An accurate X-ray spectrographic method for the analysis of a wide range of geological samples. *Geochim. Et Cosmochim. Acta* **1969**, *33*, 431–453. [[CrossRef](#)]
46. Balaram, V.; Rao, T.G. Rapid determination of REEs and trace elements in geological samples by microwave ac, Turanskaya NV (1964) The effect of climate and facies environment on the fractionation of the rare earth elements during sedimentation. *Geochem. Int.* **2003**, *1*, 951–969.
47. Taylor, S.R.; McLennan, S.M. *The Continental Crust: Its Composition and Evolution*; Blackwell Scientific Publications: London, UK, 1985; p. 312.
48. Rudnick, R.L.; Gao, S.; Holland, H.D.; Turekian, K.K. Composition of the continental crust. In *The Crust*; Elsevier: Amsterdam, The Netherlands, 2003; Volume 3, pp. 1–64.
49. Nesbitt, H.W.; Young, G.M. Early Proterozoic climates and plate motions inferred from major element chemistry of lutites. *Nature* **1982**, *299*, 715–717. [[CrossRef](#)]
50. Kutty, T.S.; Jain, S.L.; Roy Chowdhury, T. Gondwana sequence of the northern Pranhita-Godavari Valley: Its stratigraphy and vertebrate faunas. *Palaeobotanist* **1987**, *36*, 214–229.
51. Dasgupta, K. Some Contributions to the Stratigraphy of the Yerrapalli Formation, Pranhita-Godavari Valley, Deccan, India. *J. Geol. Soc. India* **1993**, *42*, 223–230.
52. Dasgupta, S.; Ghosh, P.; Gierlowski-Kordesch, E.H. A discontinuous ephemeral stream transporting mud aggregates in a continental rift basin: The Late Triassic Maleri Formation, India. *J. Sediment. Res.* **2017**, *87*, 838–865. [[CrossRef](#)]
53. Goswami, S.; Ghosh, P. Freshwater Microbialites in Early Jurassic Fluvial Strata of the Pranhita-Godavari Gondwana Basin, India. In *Limnogeology: Progress, Challenges and Opportunities, Syntheses in Limnogeology*; Springer: Berlin, Germany, 2021; pp. 549–578.
54. Cox, R.; Lowe, D.R.; Cullers, R.L. The influence of sediment recycling and basement composition on evolution of mudrock chemistry in the southwestern United States. *Geochim. Et Cosmochim. Acta* **1995**, *59*, 2919–2940. [[CrossRef](#)]
55. Folk, R.L. *Petrology of Sedimentary Rocks*; Hemphill: Austin, TX, USA, 1974.
56. Dickinson, W.R.; Beard, L.S.; Brakenridge, G.R.; Erjavec, J.L.; Ferguson, R.C.; Inman, K.F.; Knepp, R.A.; Lindberg, F.A.; Ryberg, P.T. Provenance of North American Phanerozoic sandstones in relation to tectonic setting. *Geol. Soc. Amer. Bull.* **1983**, *94*, 222–235. [[CrossRef](#)]
57. Ghosh, S.; Sarkar, S. Geochemistry of Permo-Triassic mudstone of the Satpura Gondwana basin, Central India: Clues for provenance. *Chem. Geol.* **2010**, *277*, 78–100. [[CrossRef](#)]
58. Madhavaraju, J.; Tom, M.; Lee, Y.I.; Balaram, V.; Ramasamy, S.; Carranza-Edwards, A.; Ramachandran, A. Provenance and tectonic settings of sands from Puerto Peñasco, Desemboque and Bahia Kino beaches, gulf of California, Sonora, México. *J. South Am. Earth Sci.* **2016**, *71*, 262–275. [[CrossRef](#)]
59. Chaudhuri, A.; Banerjee, S.; Chauhan, G. Compositional evolution of siliciclastic sediments recording the tectonic stability of a pericratonic rift: Mesozoic Kutch Basin, Western India. *Mar. Pet. Geol.* **2020**, *111*, 476–495. [[CrossRef](#)]
60. Chaudhuri, A.; Das, K.; Banerjee, S.; Fitzsimons, I.C.W. Detrital zircon and monazite track the source of Mesozoic sediments in Kutch to rocks of Late Neoproterozoic and Early Palaeozoic orogenies in Northern India. *Gond Res.* **2020**, *80*, 188–201. [[CrossRef](#)]
61. Chaudhuri, A.; Chatterjee, A.; Banerjee, S.; Ray, J.S. Tracing multiple sources of sediments using trace element and Nd isotope geochemistry: Provenance of the Mesozoic succession in the Kutch Basin, Western India. *Geol. Mag.* **2020**, *158*, 359–374. [[CrossRef](#)]
62. Chaudhuri, A.; Banerjee, S.; Prabhakar, N.; Das, A. The use of heavy mineral chemistry in reconstructing provenance: A case study from Mesozoic sandstones of Kutch Basin (India). *Geol. J.* **2020**, *55*, 7808–7817. [[CrossRef](#)]
63. Perri, F.; Caracciolo, L.; Cavalcante, F.; Corrado, S.; Critelli, S.; Muto, F.; Dominici, R. Sedimentary and thermal evolution of the Eocene-Oligocene mudrocks from the southwestern Thrace Basin (NE Greece). *Basin Res.* **2016**, *28*, 319–339. [[CrossRef](#)]
64. Perri, F.; Critelli, S.; Martín-Martín, M.; Montone, S.; Amendola, U. Unravelling hinterland and offshore palaeogeography from pre-to-syn-orogenic clastic sequences of the Betic Cordillera (Sierra Espuña), Spain. *Palaeogeogr. Palaeoclimatol. Palaeoecol.* **2017**, *468*, 52–69. [[CrossRef](#)]
65. Floyd, P.A.; Leveridge, B.E. Tectonic environment of the Devonian Gramscatho basin, south Cornwall: Framework mode and geochemical evidence from turbiditic sandstones. *J. Geol. Soc.* **1987**, *144*, 531–542. [[CrossRef](#)]
66. Gu, X.X.; Liu, J.M.; Zheng, M.H.; Tang, J.X.; Qi, L. Provenance and tectonic setting of the Proterozoic turbidites in Hunan, south China: Geochemical evidence. *J. Sediment. Res.* **2002**, *72*, 393–407. [[CrossRef](#)]

67. Zhu, D.; Mo, X.; Niu, Y.; Zhao, Z.; Wang, L.; Pan, G.; Wu, F. Zircon U–Pb dating and in-situ Hf isotopic analysis of Permian peraluminous granite in the Lhasa terrane, southern Tibet: Implications for Permian collisional orogeny and paleogeography. *Tectonophysics* **2009**, *469*, 48–60. [[CrossRef](#)]
68. Etemad-Saeed, N.; Hosseini-Barzi, M.; Armstrong-Altrin, J.S. Petrography and geochemistry of clastic sedimentary rocks as evidences for provenance of the Lower Cambrian Lalun Formation, Posht-e-badam block, Central Iran. *J. Afr. Earth Sci.* **2011**, *61*, 142–159. [[CrossRef](#)]
69. Wang, W.; Zhou, M.; Yan, D.; Li, J. Depositional age, provenance, and tectonic setting of the Neoproterozoic Sibao Group, southeastern Yangtze Block, South China. *Precambrian Res.* **2012**, *192*, 107–124. [[CrossRef](#)]
70. Nagarajan, R.; Armstrong-Altrin, J.S.; Kessler, F.L.; Jong, J. Petrological and geochemical constraints on provenance, paleoweathering, and tectonic setting of clastic sediments from the Neogene Lambir and Sibuti Formations, northwest Borneo. In *Sediment Provenance*; Elsevier: Amsterdam, The Netherlands, 2017; pp. 123–153.
71. Cullers, R.L. Implications of elemental concentrations for provenance, redox conditions, and metamorphic studies of shales and limestones near Pueblo, CO, USA. *Chem. Geol.* **2002**, *191*, 305–327. [[CrossRef](#)]
72. Bracciali, L.; Marroni, M.; Pandolfi, L.; Rocchi, S.; Arribas, J.; Critelli, S.; Johnsson, M.J. Geochemistry and petrography of Western Tethys Cretaceous sedimentary covers (Corsica and Northern Apennines): From source areas to configuration of margins. *Spec. Pap. Geol. Soc. Am.* **2007**, *420*, 73–93.
73. Mongelli, G.; Critelli, S.; Perri, F.; Sonnino, M.; Perrone, V. Sedimentary recycling, provenance and paleoweathering from chemistry and mineralogy of Mesozoic continental redbed mudrocks, Peloritani Mountains, Southern Italy. *Geochem. J.* **2006**, *40*, 197–209. [[CrossRef](#)]
74. Nesbitt, H.W.; Young, G.M. Prediction of some weathering trends of plutonic and volcanic rocks based on thermodynamic and kinetic considerations. *J. Geol.* **1984**, *48*, 1523–1534. [[CrossRef](#)]
75. McLennan, S.M.; Bock, B.; Hemming, S.R.; Hurowitz, J.A.; Lev, S.M.; McDaniel, K.D. The roles of provenance and sedimentary processes in the geochemistry of sedimentary rocks. In *Geochemistry of Sediments and Sedimentary Rocks: Evolutionary Considerations to Mineral Deposit-Forming Environments*; Geological Association of Canada: St. John, NL, Canada, 2003; Volume 4, pp. 7–38.
76. Reynard, B.; Lécuyer, C.; Grandjean, P. Crystal-chemical controls on rare earth element concentrations in fossil biogenic apatites and implications for paleoenvironmental reconstructions. *Chem. Geol.* **1999**, *155*, 233–241. [[CrossRef](#)]
77. Ryan, K.M.; Williams, D.M. Testing the reliability of discrimination diagrams for determining the tectonic depositional environment of ancient sedimentary basins. *Chem. Geol.* **2007**, *242*, 103–125. [[CrossRef](#)]
78. Verma, S.P.; Armstrong-Altrin, J.S. New multi-dimensional diagrams for tectonic discrimination of siliciclastic sediments and their application to Precambrian basins. *Chem. Geol.* **2013**, *355*, 117–133. [[CrossRef](#)]
79. Maravelis, A.G.; Offler, R.; Pantopoulos, G.; Collins, W.J. Provenance and tectonic setting of the Early Permian sedimentary succession in the southern edge of the Sydney Basin, eastern Australia. *Geol. J.* **2020**, *4*, 2258–2276.
80. Long, X.; Sun, M.; Yuan, C.; Kröner, A.; Hu, A. Zircon REE patterns and geochemical characteristics of Paleoproterozoic anatectic granite in the northern Tarim Craton, NW China: Implications for the reconstruction of the Columbia supercontinent. *Precambrian Res.* **2012**, *222*, 474–487.
81. McLennan, S.M.; Taylor, S.R. Sedimentary rocks and crustal evolution: Tectonic setting and secular trends. *J. Geol.* **1991**, *99*, 1–21. [[CrossRef](#)]
82. Rudra, D.K.; Maulik, P.K. Lower Jurassic Kota Limestone of India. *Glob. Geol. Rec. Lake Basins* **1994**, *1*, 185–191.
83. Goswami, S.; Gierlowski-Kordesch, E.H.; Ghosh, P. Sedimentology of the Early Jurassic limestone beds of the Kota Formation: Record of carbonate wetlands in a continental rift basin of India. *J. Paleolimnol.* **2018**, *59*, 21–28.